

Randomized Rank-Revealing QLP for Low-Rank Matrix Decomposition

Maboud F. Kaloorazi[†], Kai Liu[‡], Jie Chen[‡], Rodrigo C. de Lamare[§], and Susanto Rahardja[‡]

[†] School of Electronic Engineering, Xi'an Shiyou University, Xi'an, China

[‡] CIAIC, Northwestern Polytechnical University, Xi'an, China

[§] CETUC, Pontifical Catholic University of Rio de Janeiro, Brazil

Abstract—The pivoted QLP decomposition is computed through two consecutive pivoted QR decompositions, and provides an approximation to the singular value decomposition. This work is concerned with a partial QLP decomposition of low-rank matrices computed through randomization, termed Randomized Unpivoted QLP (RU-QLP). Like pivoted QLP, RU-QLP is rank-revealing and yet it utilizes random column sampling and the unpivoted QR decomposition. The latter modifications allow RU-QLP to be highly parallelizable on modern computational platforms. We provide an analysis for RU-QLP, deriving bounds in spectral and Frobenius norms on: i) the rank-revealing property; ii) principal angles between approximate subspaces and exact singular subspaces and vectors; and iii) low-rank approximation errors. Effectiveness of the bounds is illustrated through numerical tests. We further use a modern, multicore machine equipped with a GPU to demonstrate the efficiency of RU-QLP. Our results show that compared to the randomized SVD, RU-QLP achieves a speedup of up to 7.1 times on the CPU and up to 2.3 times with the GPU.

Index Terms—Randomized methods, singular value decomposition, rank-revealing decomposition, pivoted QLP, low-rank approximation, principal angles, high-performance computing.

I. INTRODUCTION

Randomized methods for low-rank matrix approximation and factorization have many applications in signal processing, machine learning, and modern data analysis. This is in particular motivated by ubiquitousness of large-scale matrices with low-rank structure in applications such as weather forecast [1], principal components regression [2], latent variable models [3], image deblurring [4], background modeling [5], deep learning classification and regression [6], large-scale multiple-antenna systems [7], community detection [8], Stokes flow equations [9], subspace estimation and tracking [10], covariance estimation [11], Gaussian processes [12], and learning mixture models [13].

Classical, deterministic matrix decompositions such as the SVD (singular value decomposition) [14], the pivoted QR [15], [14] and QLP [16] decompositions are extensively used for low-rank factorization tasks. However, they are in general faced with two daunting challenges, particularly when applied in modern applications and machines: first, they need a large number of arithmetic operations; and second, their communication costs, that is, moving data between the slow and fast memory or between processors [17]–[19] are expensive.

Randomized methods [20], [21], [22], [5], [23], [24], [25], [26], on the other hand, provide approximations to the deterministic decompositions. They aim to address the foregoing

bottlenecks at the expense of accuracy: they are arithmetically more efficient, can leverage the parallel structure in modern machines, but less accurate. The latter is justified as optimality in accuracy is not needed in many applications. Randomized methods make use of deterministic decompositions in their computational procedures. Their computations involve three steps: i) reducing the dimension of the original input matrix through a random matrix multiplication; ii) performing the SVD, the pivoted QR or QLP decomposition; and iii) constructing the factorization through piecing back together the components. Due to the second step, depending on the size of the data and application in hand, randomized methods may still suffer from the bottleneck associated with the communication cost. Recently, however, a randomized method, called here Randomized Unpivoted QLP (RU-QLP), was proposed in [21] that copes with this issue; it makes use of only the unpivoted QR decomposition, which requires less communication among all deterministic decompositional methods.

A. Our Contributions

Our paper focuses on the RU-QLP decomposition, an approximation of truncated pivoted QLP computed via random sampling and the highly parallelizable unpivoted QR factorization. It provides an in-depth analysis of the method, furnishing bounds for i) the rank-revealing property, ii) principal angles between approximate subspaces and exact singular subspaces and vectors, and iii) low-rank approximation errors. There are, however, differences between the analysis of this paper and the one presented in the original paper. First, the proof technique of our results presented here is different, yet simpler and easier to follow. Our analysis can be viewed as a systematic treatment of randomized methods for low-rank matrix factorization and hence can be adopted by other methods of this class in order to derive error bounds. However, an SVD-like factorization enables deriving more bounds; see Remarks 1 and 3.

Second, all bounds presented here are different, some of which are missing in the original paper. To be specific, we derive bounds for the following, most of which are in terms of both spectral and Frobenius norm:

- All principal angles between the approximate left and right subspaces and i) the singular subspaces and ii) the subspaces spanned by the individual singular vectors.
- The errors incurred by the low-rank approximations constructed through the estimated bases for both the right and left singular vectors.

Third, we provide an empirical evaluation of the derived bounds, which brings an insight into characteristics and behavior of RU-QLP as well as the tightness of the bounds.

In addition, we implement RU-QLP and several competing randomized methods on an advanced, multicore machine equipped with a GPU and discuss their performance behaviors.

B. Overview

In Section II, we describe the notations used in our paper, and briefly review the related deterministic and randomized methods. In Section III, we describe RU-QLP in detail, its intuition and relation to the classical method of orthogonal iteration, as well as its computational cost. Section IV establishes a canonical theoretical analysis of RU-QLP, shedding light on its characteristics. Section V presents the runtime results of RU-QLP and several randomized methods implemented on a hybrid GPU-based architecture, as well as those of empirical evaluation of the developed bounds using several matrices. Concluding remarks are given in Section VI.

II. BACKGROUND

A. Notation and Conventions

This section summarizes our notation and conventions.

We consider a real $m \times n$ matrix \mathbf{A} with $m \geq n$. We denote the i th column of \mathbf{A} by \mathbf{a}_i , and the i th largest and the minimum singular value of \mathbf{A} by $\sigma_i(\mathbf{A})$ and $\sigma_{\min}(\mathbf{A})$, respectively. We assume that the singular values of \mathbf{A} are arranged in a decreasing order, and there is a well-defined gap between $\sigma_k(\mathbf{A})$ and $\sigma_{k+1}(\mathbf{A})$, that is, \mathbf{A} has rank k . For a symmetric matrix \mathbf{A} , $\lambda_i(\mathbf{A})$ denotes the i th largest eigenvalue.

The symbol $\|\cdot\|_2$ denotes the spectral norm (or 2-norm), $\|\cdot\|_F$ the Frobenius norm, $\|\cdot\|$ any unitary invariant norm, and $\|\cdot\|_{2,F}$ holds for both the spectral and Frobenius norms. \mathbf{I} denotes an identity matrix whose dimension is determined by the context, and the dagger \dagger denotes the Moore-Penrose inverse. $\mathcal{R}(\mathbf{A})$ denotes the numerical range and $\mathcal{N}(\mathbf{A})$ the null space of \mathbf{A} . `randn()` generates a random matrix whose entries have a standard Gaussian distribution, `orth(A)` constructs a set of orthonormal basis for the columns of \mathbf{A} , and `qr(A)` computes the unpivoted QR factorization. The notation $[\mathbf{A}]_k$ denotes the optimal rank- k approximation of \mathbf{A} , and \mathbb{E} denotes the expected value.

B. Deterministic Methods

Let $\mathbf{A} \in \mathbb{R}^{m \times n}$ be our rank- k input matrix. The (thin) SVD [14, Section 2.5.4] decomposes \mathbf{A} into two orthonormal matrices \mathbf{U} and \mathbf{V} and one diagonal matrix $\mathbf{\Sigma}$:

$$\mathbf{A} = \mathbf{U}\mathbf{\Sigma}\mathbf{V}^T = [\mathbf{U}_k \quad \mathbf{U}_\perp] \begin{bmatrix} \mathbf{\Sigma}_k & \mathbf{0} \\ \mathbf{0} & \mathbf{\Sigma}_\perp \end{bmatrix} \begin{bmatrix} \mathbf{V}_k^T \\ \mathbf{V}_\perp^T \end{bmatrix}. \quad (1)$$

The SVD is viewed as the optimal decomposition of any matrix, as it furnishes information on singular values and four fundamental subspaces of the matrix. In particular, the columns of $\mathbf{U}_k \in \mathbb{R}^{m \times k}$, $\mathbf{U}_\perp \in \mathbb{R}^{m \times (n-k)}$, $\mathbf{V}_k \in \mathbb{R}^{n \times k}$ and $\mathbf{V}_\perp \in \mathbb{R}^{n \times (n-k)}$ span $\mathcal{R}(\mathbf{A})$, $\mathcal{N}(\mathbf{A}^T)$, $\mathcal{R}(\mathbf{A}^T)$ and $\mathcal{N}(\mathbf{A})$, respectively. $\mathbf{\Sigma}_k$ contains the first k and $\mathbf{\Sigma}_\perp$ the remaining

$n - k$ singular values σ_i . The SVD constitutes an optimal choice in constructing a rank- r approximation \mathbf{B} to \mathbf{A} [27, Chapter 1, Theorem 4.32] such that:

$$\operatorname{argmin}_{\operatorname{rank}(\mathbf{B}) \leq r} \|\mathbf{A} - \mathbf{B}\|_{2,F} = \|\mathbf{\Sigma}_{r+1}\|_{2,F},$$

where $\|\mathbf{\Sigma}_{r+1}\|_2 = \sigma_{r+1}$, and $\|\mathbf{\Sigma}_{r+1}\|_F = \left(\sum_{i=r+1}^n \sigma_i^2\right)^{1/2}$. The classical bidiagonalization method [14, Section 8.6.2], [18] is usually leveraged to compute the SVD, which involves two main steps. First, the matrix \mathbf{A} is reduced to a bidiagonal form, and then the bidiagonal matrix is transformed to a diagonal matrix via, e.g, the QR algorithm.

The pivoted QR decomposition [14, Section 5.4.1], or rank-revealing QR decomposition [15], [28], [29], [30, Section 2.4.3] factorizes \mathbf{A} into a permutation matrix $\mathbf{\Pi}$, an orthonormal matrix \mathbf{Q} , and an upper triangular matrix \mathbf{R} :

$$\mathbf{A}\mathbf{\Pi} = \mathbf{Q}\mathbf{R} = [\mathbf{Q}_1 \quad \mathbf{Q}_2] \begin{bmatrix} \mathbf{R}_{11} & \mathbf{R}_{12} \\ \mathbf{0} & \mathbf{R}_{22} \end{bmatrix}.$$

Pivoted QR is computed by applying Householder reflections to \mathbf{A} in which the columns with largest 2-norms are exchanged with other columns before the reduction proceeds. The columns of \mathbf{Q}_1 and \mathbf{Q}_2 span respectively $\mathcal{R}(\mathbf{A})$ and $\mathcal{N}(\mathbf{A}^T)$, and the diagonals of \mathbf{R} are approximations to $\sigma_i(\mathbf{A})$. $\mathbf{R}_{11} \in \mathbb{R}^{k \times k}$ is well-conditioned, and the blocks of \mathbf{R} satisfies

$$\begin{aligned} \sigma_{\min}(\mathbf{R}_{11}) &\geq \sigma_k(\mathbf{A})/p(n, k), \\ \sigma_1(\mathbf{R}_{22}) &\leq \sigma_{k+1}(\mathbf{A})q(n, k), \end{aligned} \quad (2)$$

where $p(n, k)$ and $q(n, k)$ are low degree polynomials in n and k . Pivoted QR, despite being computationally more efficient than the SVD, suffers from two shortcomings: i) it gives fuzzy singular-value estimates; and ii) it does not explicitly provide orthogonal bases for $\mathcal{R}(\mathbf{A}^T)$ and $\mathcal{N}(\mathbf{A})$.

UTV decompositions [27, Chapter 5, Section 4] are a class of rank-revealing methods that factorize the matrix \mathbf{A} into three components:

$$\mathbf{A} = \mathbf{U}\mathbf{T}\mathbf{V}^T,$$

where \mathbf{U} and \mathbf{V} are orthogonal, and \mathbf{T} is upper or lower triangular. The computation of UTV decompositions involves two main steps: an initial unpivoted QR factorization followed by deflation steps (or rank-revealing step) in which the largest, or the smallest singular values are extracted one at a time. The UTVs provide information on $\mathcal{R}(\mathbf{A}^T)$ and $\mathcal{N}(\mathbf{A})$ as well.

The pivoted QLP decomposition introduced by Stewart [16], is viewed as an approximate SVD. It is computed through two consecutive pivoted QR factorizations, first on \mathbf{A} , then on \mathbf{R}^T :

$$\mathbf{A}\mathbf{\Pi} = \mathbf{Q}\mathbf{R}, \quad \mathbf{R}^T\mathbf{\dot{\Pi}} = \mathbf{\dot{P}}\mathbf{\dot{L}}^T, \quad (3)$$

which gives $\mathbf{A} = \mathbf{Q}\mathbf{\dot{\Pi}}\mathbf{\dot{L}}^T\mathbf{\Pi}^T$. The matrices $\mathbf{Q}\mathbf{\dot{\Pi}}$ and $\mathbf{\Pi}\mathbf{\dot{P}}$ are orthogonal, providing bases for the spaces spanned by the columns and rows of \mathbf{A} , respectively. $\mathbf{\dot{L}}$ is lower triangular and, as demonstrated by Stewart, its diagonals (the L-values) give better approximations to $\sigma_i(\mathbf{A})$ than the diagonals of \mathbf{R} (the R-values). In computing pivoted QLP, the first permutation $\mathbf{\Pi}$ is important, whereas the second one $\mathbf{\dot{\Pi}}$ is not always necessary [16], [31]. This principle has been leveraged for developing RU-QLP, as will be discussed later.

C. Shortcomings of Deterministic Methods

1) *Arithmetic cost*: Arithmetic operations required by deterministic methods to factorize \mathbf{A} are of order mn^2 . This is the cost of a *full* factorization, giving all relevant information. Considering large-scale matrices in modern applications, this is obviously prohibitively expensive. However, if a rank k factorization is desired, deterministic methods need $\mathcal{O}(mnk)$ operations to give the truncated version. These methods, however, need to repeatedly *access* the data, which brings us to a more important cost associated with decomposition methods on modern computers, namely the communication cost.

2) *Communication cost*: The cost of transferring data between different processors or between different levels of the memory hierarchy is defined as the communication cost. On advanced parallel machines, it is substantially more expensive than the arithmetic cost in terms of time as well as energy consumption [19]. The communication cost is associated with the use of level-1, 2 and 3 BLAS (the Basic Linear Algebra Subprograms) routines, a set of standard routines for performing basic linear algebra operations [18], [32]. Memory-bound level-1 and level-2 BLAS routines cannot attain high performance on modern computers. However, level-3 BLAS routines are CPU-bound, which enables harnessing the parallel structure of modern machines.

To approximate the SVD or/and UTV decompositions, Krylov subspace methods, such as the Lanczos algorithm, are used [33], [34]. A large portion of operations of such methods are performed in level-1 and level-2 BLAS. Pivoted QR needs to compute the 2-norm of the matrix columns and swap them, and hence nearly half of its operations are in level-3 BLAS. While, most operations of the unpivoted QR decomposition are in level-3 BLAS, meaning that it is *communication-friendly*, and can be efficiently implemented on parallel machines. Recently, randomized techniques have been used to develop block Krylov subspace methods [35]–[37] and “communication-avoiding” pivoted QR decompositions [17], [38], [39].

D. Randomized Methods

Methods based on randomized sampling offer efficient and compatible approximations to traditional decompositions; they are efficient in arithmetic operations, and can harness modern computing devices. Efficiency is achieved due to transforming the input matrix to a lower dimensional space in which only *important* features are kept. This in turn leads to less accurate approximations. However, in many practical applications, the optimality is not necessary. In addition, there are some techniques, such as the power method, that substantially improve the quality of approximations in exchange of extra computations. The above factors make the randomized methods very attractive for processing low-rank matrices.

The line of research on randomized methods that culminated in RU-QLP [21] started with [40], and hence we discuss such methods. We refer to [20, Section 2] and [41, Section 2.4], [42], [43] for other classes of randomized methods. The general strategy underlying the randomized methods involves the following steps:

Step 1: The input matrix is transformed to a lower-dimensional space by utilizing a random matrix, thereby giving a smaller matrix formed by the linear combinations of rows or columns. Then orthonormal bases are obtained through the Gram–Schmidt process [30], [44, Section 2.3.4] or Householder reflections [14], [45], [46, 5.1.2].

Step 2: Orthonormal bases are applied to the original matrix, and the SVD or pivoted QR or QLP decomposition of the reduced-size matrix is computed.

Step 3: The orthogonal and diagonal or (upper/lower) triangular components are pieced back together and form the final approximation.

The random matrix used in Step 1 is usually standard Gaussian; see [42, Section 3.9] for a discussion about other choices. The major difference in computational procedure of the randomized methods, however, appears in Step 2. The works in [40] and [20] make use of the SVD, where the resulting method of the latter is called the “randomized SVD” (R-SVD). The error analyses presented are different. Gu [22] uses the truncated SVD in Step 2. His error analysis is different from the mentioned works, and the bounds explicitly contain the oversampling parameter. The work in [5] presents a two-sided R-SVD. It uses the truncated SVD, and the proof techniques are based on [22]. Saibaba [24] presents a new analysis for R-SVD. In particular, he develops a set of bounds for canonical angles between approximate subspaces and exact singular subspaces and individual singular vectors. The works in [23], and [25] are based on the two-sided R-SVD, but the difference is that the former employs pivoted QR, and the latter pivoted QLP. The work in [47] presents a randomized QLP method by supplanting the SVD in R-SVD [20] with pivoted QLP. The method in [26] make use of pivoted QLP, and the authors provide bounds for approximate singular values, canonical angles between the exact and approximate subspaces, and the low-rank approximation error.

The foregoing methods apply the SVD, pivoted QR or pivoted QLP to compute the low-rank factorization of an input matrix. Each method gives three factors: two matrices with orthonormal columns and one matrix with diagonal or triangular structure containing the approximate singular values. As stated, the execution of these methods may bring substantial communication cost when processing large-scale matrices, due to the use of level-1 and level-2 BLAS routines. RU-QLP [21], however, uses the unpivoted QR factorization in Step 2, whose operations are almost entirely in level-3 BLAS. This enables RU-QLP to take advantage of advanced computer architectures and hence to be implemented more efficiently compared to any other randomized method. In the next section, we describe RU-QLP, the intuition behind its development, as well as some theory explaining the relationship between RU-QLP and the classical Orthogonal Iteration [14, Section 8.2.4].

We add that there is a class of randomized block Krylov subspace methods, e.g., [48], [49], that provide low-rank approximations; they approximate the left invariant subspace of a matrix and use its orthogonal projection to construct the approximation. They do not provide information on the right invariant subspace nor the singular values. If only a low-rank approximation is desired, these methods can also be used.

III. RANDOMIZED UNPIVOTED QLP (RU-QLP)

A. Computation of RU-QLP

Given the matrix \mathbf{A} with rank $k \geq 1$, and $d = k + p < n$, where p is an oversampling parameter, RU-QLP is computed as follows:

1. Generate a standard Gaussian matrix $\Phi \in \mathbb{R}^{m \times d}$.
2. Compress the matrix \mathbf{A} via Φ to obtain $\mathbf{A}^T \Phi$.
3. Form a matrix of orthonormal bases $\bar{\mathbf{P}} = \text{orth}(\mathbf{A}^T \Phi)$.
4. Compute the matrix product $\mathbf{A}\bar{\mathbf{P}}$, and carry out two unpivoted QR factorizations: $[\mathbf{Q}, \mathbf{R}] = \text{qr}(\mathbf{A}\bar{\mathbf{P}})$, and $[\tilde{\mathbf{P}}, \tilde{\mathbf{R}}] = \text{qr}(\mathbf{R}^T)$.
5. Construct the rank- d approximation $\hat{\mathbf{A}} = \mathbf{Q}\mathbf{L}\mathbf{P}^T$, where $\mathbf{Q} \in \mathbb{R}^{m \times d}$ approximates $\mathcal{R}(\mathbf{A})$, $\mathbf{L} \triangleq \tilde{\mathbf{R}}^T \in \mathbb{R}^{d \times d}$ is lower triangular whose elements on the diagonal are approximations to the first d singular values of \mathbf{A} , and whose leading block of size $k \times k$ reveals the rank k of \mathbf{A} , and $\mathbf{P} \triangleq \tilde{\mathbf{P}}\bar{\mathbf{P}} \in \mathbb{R}^{m \times d}$ approximates $\mathcal{R}(\mathbf{A}^T)$. RU-QLP is presented in Algorithm 1.

Algorithm 1 Randomized Unpivoted QLP (RU-QLP)

Input: $\mathbf{A} \in \mathbb{R}^{m \times n}$, and $1 \leq k \leq d < n$.
Output: $\mathbf{Q} \in \mathbb{R}^{m \times d}$ and $\mathbf{P} \in \mathbb{R}^{n \times d}$ with orthonormal columns, and lower triangular $\mathbf{L} \in \mathbb{R}^{d \times d}$ that form an approximation $\hat{\mathbf{A}} = \mathbf{Q}\mathbf{L}\mathbf{P}^T$.

- 1: **function** RU_QLP(\mathbf{A} , d)
- 2: $\Phi = \text{randn}(m, d)$
- 3: $\bar{\mathbf{P}} = \text{orth}(\mathbf{A}^T \Phi)$
- 4: $[\mathbf{Q}, \mathbf{R}] = \text{qr}(\mathbf{A}\bar{\mathbf{P}})$
- 5: $[\tilde{\mathbf{P}}, \tilde{\mathbf{R}}] = \text{qr}(\mathbf{R}^T)$
- 6: **return** \mathbf{Q} ; $\mathbf{P} \triangleq \tilde{\mathbf{P}}\bar{\mathbf{P}}$; $\mathbf{L} \triangleq \tilde{\mathbf{R}}^T$
- 7: **end function**

B. Improvement and numerical stability

To ameliorate the approximation quality, particularly when the singular values of the input matrix do not decay relatively fast, we use the power iteration technique: it replaces \mathbf{A}^T in Step 3 of Algorithm 1 with $\mathbf{A}_q = (\mathbf{A}^T \mathbf{A})^q \mathbf{A}^T$, a closely related matrix whose singular values decay more quickly. Here $q \geq 1$ is the power method factor. The power iteration also affects the convergence of the bases of approximate left and right invariant subspaces: the approximate subspaces converge to invariant subspaces at a rate proportional to $(\sigma_{k+1}/\sigma_k)^q$.

There is, however, a concern regarding the computation of \mathbf{A}_q in floating point arithmetic: it is prone to rounding errors, which will lead to loss of information associated with some small singular values. To be specific, considering the machine precision $\epsilon_{\text{machine}}$, the singular components less than $\sigma_1 \epsilon_{\text{machine}}^{1/(2q+1)}$ will be lost; see [21, Section V-D] for an example. Thus, to have better numerical accuracy, Algorithm 2 needs to be used to compute $\bar{\mathbf{P}}$ in Algorithm 1, where the columns of the sample matrix between each application of \mathbf{A} and \mathbf{A}^T are orthonormalized [20]–[22]. A point to bear in mind is that since orthonormalization incurs extra cost, it is recommended to be used once in every few iterations, as to balance numerical stability and efficiency.

Algorithm 2 Power Iteration and Orthogonalization

Input: $\mathbf{A} \in \mathbb{R}^{m \times n}$, $\Phi \in \mathbb{R}^{m \times d}$, and $q \geq 1$.
Output: $\bar{\mathbf{P}} \in \mathbb{R}^{n \times d}$ with orthonormal columns.

- 1: **function** PI_ORTH(\mathbf{A} , Φ , q)
- 2: $\bar{\mathbf{P}} = \text{orth}(\mathbf{A}^T \Phi)$
- 3: **for** $i = 1, \dots, q$
- 4: $\mathbf{B} = \mathbf{A}\bar{\mathbf{P}}$; $\bar{\mathbf{P}} = \text{orth}(\mathbf{B})$
- 5: $\mathbf{B} = \mathbf{A}^T \bar{\mathbf{P}}$; $\bar{\mathbf{P}} = \text{orth}(\mathbf{B})$
- 6: **end for**
- 7: **return** $\bar{\mathbf{P}}$
- 8: **end function**

C. Intuition and relation to Orthogonal Iteration

The pivoted QLP decomposition is computed with two consecutive pivoted QR factorizations, first on \mathbf{A} , then on \mathbf{R}^T . The first pivoting is important, as Stewart points out [16], but the main purpose of the second pivoting is to ensure that the L-values are arranged in a decreasing order. In another words, if the space spanned by the first k columns of \mathbf{Q} (3) furnishes a good approximation to the left invariant subspace of \mathbf{A} and thus giving a well-conditioned leading block of order k in the R factor that reveals the rank of \mathbf{A} , then the second pivoting can be circumvented. To connect it to RU-QLP, we show that the first k columns of \mathbf{Q} obtained by the unpivoted QR factorization on $\mathbf{A}\bar{\mathbf{P}}$ in fact gives a good approximation to $\mathcal{R}(\mathbf{A})$. We further show that the leading block of the R factor reveals the rank of \mathbf{A} . This is in essence due to the fact that $\bar{\mathbf{P}}$ approximates $\mathcal{R}(\mathbf{A}^T)$, and a high-quality approximation is given when the power iteration is used.

Orthogonal Iteration [14, Section 8.2.4] is a generalization of the power method. It is used to compute the dominant invariant subspaces of a matrix. Let $\mathbf{A} \in \mathbb{R}^{n \times n}$ and $\mathbf{Q}^{(0)}$ be $m \times k$ with orthonormal columns. The following orthogonal iteration procedure produces a sequence of $\mathbf{Q}^{(m)}$:

```

for  $m = 1, 2, \dots$ 
   $\mathbf{Z}^{(m)} = \mathbf{A}\mathbf{Q}^{(m-1)}$ 
   $\mathbf{Z}^{(m)} = \mathbf{Q}^{(m)}\mathbf{R}^{(m)}$ 
end

```

Under the assumption that the eigenvalues of \mathbf{A} are arranged in decreasing order, and that the largest k eigenvalues are separated from the remainder of the spectrum, $\mathcal{R}(\mathbf{Q}^{(m)})$ converges to the dominant left invariant subspace of \mathbf{A} as $m \rightarrow \infty$. If \mathbf{A} is real, then the diagonal entries of \mathbf{R} converge to the dominant eigenvalues.

Unlike the orthogonal iteration method, we construct $\bar{\mathbf{P}}$ through random sampling of \mathbf{A} 's rows. However, we observe that the Q and R factors of the QR factorization of $\mathbf{A}\bar{\mathbf{P}}$ reveal similar information as those of orthogonal iteration: an approximate basis for the invariant subspace and approximate singular values, respectively. These results are improved when the power iteration is used in forming $\bar{\mathbf{P}}$. It is this principle that is leveraged in developing RU-QLP.

Remark 1: It is possible to turn RU-QLP to an SVD-like decomposition by computing an SVD of $\mathbf{R} = \bar{\mathbf{U}}\bar{\Sigma}\bar{\mathbf{V}}$. This, however, can be done entirely using unpivoted QR, due to the method of QR-based Dynamically Weighted Halley (QDWH)-

SVD [50], a spectral divide and conquer method that computes the SVD of a matrix via its polar decomposition. On \mathbf{R} , this method, however, needs up to $52d^3$ operations, as opposed to $4d^3/3$ or $2d^3$ operations for an unpivoted QR, which clearly demands more resources.

D. Computational Cost

The number of arithmetic operations required to compute RU-QLP is as follows:

- Forming the matrix Φ : $\mathcal{O}(md)$;
- Forming $\mathbf{A}^T \Phi$: $\mathcal{O}(mnd)$;
- Computing \mathbf{P} : $\mathcal{O}(nd^2)$;
- Forming $\mathbf{A}\mathbf{P}$: $\mathcal{O}(mnd)$;
- Computing \mathbf{Q} and \mathbf{R} : $\mathcal{O}(md^2)$;
- Computing $\bar{\mathbf{P}}$ and $\bar{\mathbf{R}}$: $\mathcal{O}(d^3)$;
- Forming \mathbf{P} : $\mathcal{O}(nd^2)$.

The dominant cost is $\mathcal{C} = \mathcal{O}(mnd)$. If the input matrix \mathbf{A} is stored out-of-core, RU-QLP is computed by two passes over \mathbf{A} . If the power iteration is used, as to improve the approximation quality, RU-QLP needs $2q + 2$ passes over \mathbf{A} , and $(q + 1)\mathcal{C}$ operations. In addition, if \mathbf{A} is sparse with s non-zero entries, computing RU-QLP costs $\mathcal{O}(sd)$.

As discussed earlier, in modern computer architectures, the cost of communication [17]–[19] in performing decompositional methods dominates the arithmetic cost. This is associated with level-1, 2 and 3 BLAS routines. The methods that are rich in level-3 BLAS, i.e., matrix-matrix multiplications, attain higher performance, as they exploit the data locality in modern architectures. In contrast to the SVD, and pivoted QR, unpivoted QR can be computed almost entirely using level-BLAS 3 routines, thereby lending itself much easier to parallel implementation. This in turn makes RU-QLP the fastest randomized method, as will be shown in Section V-A.

IV. THEORETICAL ANALYSIS

We first define a few terms that are used in our results. Let the input matrix \mathbf{A} have an SVD as in (1), and $\Phi_1 \in \mathbb{R}^{k \times d}$ and $\Phi_2 \in \mathbb{R}^{(m-k) \times d}$ be defined as follows:

$$\mathbf{U}^T \Phi = \begin{bmatrix} \mathbf{U}_k^T \Phi \\ \mathbf{U}_\perp^T \Phi \end{bmatrix} \triangleq \begin{bmatrix} \Phi_1 \\ \Phi_2 \end{bmatrix}. \quad (4)$$

Let $\delta_i \triangleq \frac{\sigma_{k+1}}{\sigma_i}$, for $i = 1, \dots, k$, and $\gamma \triangleq \sigma_n / \sigma_1$. Let further $\mathbf{A}\bar{\mathbf{P}}$ and its QR factorization be written as:

$$\mathbf{A}\bar{\mathbf{P}} = [\mathbf{A}\bar{\mathbf{P}}_1 \quad \mathbf{A}\bar{\mathbf{P}}_2] = [\mathbf{Q}_1 \quad \mathbf{Q}_2] \begin{bmatrix} \mathbf{R}_{11} & \mathbf{R}_{12} \\ \mathbf{0} & \mathbf{R}_{22} \end{bmatrix}, \quad (5)$$

where $\bar{\mathbf{P}}_1 \in \mathbb{R}^{n \times k}$ and $\mathbf{Q}_1 \in \mathbb{R}^{m \times k}$, giving

$$\begin{aligned} \mathbf{A}\bar{\mathbf{P}}_1 &= \mathbf{Q}_1 \mathbf{R}_{11}, \\ \mathbf{A}\bar{\mathbf{P}}_2 &= \mathbf{Q}_1 \mathbf{R}_{12} + \mathbf{Q}_2 \mathbf{R}_{22}. \end{aligned} \quad (6)$$

A. \mathbf{R} Reveals the Numerical Rank of \mathbf{A}

We first show that the R factor (5) generated by an unpivoted QR factorization in the RU-QLP computational procedure reveals the rank of \mathbf{A} . Our results parallel those of deterministic rank-revealing decompositions (2).

Theorem 1: Let \mathbf{A} be an $m \times n$ matrix whose SVD is defined in (1). Let \mathbf{R} be generated by RU-QLP and partitioned as in (5). Then

$$\sigma_k \geq \sigma_k(\mathbf{R}_{11}) \geq \frac{\sigma_k}{\sqrt{1 + \delta_k^{4q+4} \|\Phi_2 \Phi_1^\dagger\|_2^2}}, \quad (7)$$

$$\|\mathbf{R}_{22}\|_{2,F} \leq \left(1 + \frac{\delta_k^{2q+1} \|\Phi_2 \Phi_1^\dagger\|_2}{1 + \gamma^{4q+4} \|\Phi_2 \Phi_1^\dagger\|_2^2} \right) \|\Sigma_\perp\|_{2,F}. \quad (8)$$

Proof. The proof is given in Appendix A.

Theorem 1 makes it explicit that the convergence of $\sigma_k(\mathbf{R}_{11})$ and $\|\mathbf{R}_{22}\|_{2,F}$ is governed by the ratio $\delta_k = \frac{\sigma_{k+1}}{\sigma_k}$, or simply the gap in the spectrum. Provided that $\sigma_k \gg \sigma_{k+1}$ fast convergence is expected.

Corollary 1: Under the hypotheses of Theorem 1, let further \mathbf{L} be the middle factor in the RU-QLP decomposition. Then, for $i = 1, \dots, k$,

$$\sigma_i \geq \sigma_i(\mathbf{L}) \geq \frac{\sigma_i}{\sqrt{1 + \delta_k^{4q+4} \|\Phi_2 \Phi_1^\dagger\|_2^2}}.$$

The above relation follows due to [51, Theorem 2.1]. Tighter and more complicated bounds for $\sigma_i(\mathbf{L})$ can be obtained using the techniques in [31].

B. Bounds for Principal Angles

Canonical or principal angles are used to measure the closeness of any two subspaces [52], [53]. The ranges of \mathbf{Q} and \mathbf{P} generated by RU-QLP approximate the ranges of \mathbf{U}_k and \mathbf{V}_k , respectively. Let $\theta_i = \angle(\mathcal{R}(\mathbf{Q}), \mathcal{R}(\mathbf{U}_k))$ and $\phi_i = \angle(\mathcal{R}(\mathbf{P}), \mathcal{R}(\mathbf{V}_k))$ be the angles between the approximate and exact subspaces. The following results show how accurate the approximations are.

Theorem 2: Let \mathbf{A} be an $m \times n$ matrix whose SVD is defined in (1). Let \mathbf{A} have a RU-QLP decomposition as described in Section III. Then

$$\sin \theta_i \leq \frac{\delta_i^{2q+2} \|\Phi_2 \Phi_1^\dagger\|_2}{\sqrt{1 + \delta_i^{4q+4} \|\Phi_2 \Phi_1^\dagger\|_2^2}}, \quad (9)$$

$$\sin \phi_i \leq \frac{\delta_i^{2q+1} \|\Phi_2 \Phi_1^\dagger\|_2}{\sqrt{1 + \delta_i^{4q+2} \|\Phi_2 \Phi_1^\dagger\|_2^2}}. \quad (10)$$

Proof. The proof is presented in Appendix B.

Theorem 2 makes two points clear. First, θ_i and ϕ_i approach zero at a rate proportional to $(\sigma_{k+1}/\sigma_i)^q$. Provided that $\sigma_i > \sigma_{k+1}$, as the power factor q increases, the approximate subspaces become more accurate. Through numerical tests we show that this holds true. Second, θ_i is smaller than ϕ_i . This is because the computation of \mathbf{Q} requires $\bar{\mathbf{P}}$, which forms \mathbf{P} , and hence one more step of iteration.

Corollary 2: Under the hypotheses of Theorem 2, we have

$$\begin{aligned} \cos \theta_i &\geq \frac{1}{\sqrt{1 + \delta_i^{4q+4} \|\Phi_2 \Phi_1^\dagger\|_2^2}}, \quad \tan \theta_i \leq \delta_i^{2q+2} \|\Phi_2 \Phi_1^\dagger\|_2, \\ \cos \phi_i &\geq \frac{1}{\sqrt{1 + \delta_i^{4q+2} \|\Phi_2 \Phi_1^\dagger\|_2^2}}, \quad \tan \phi_i \leq \delta_i^{2q+1} \|\Phi_2 \Phi_1^\dagger\|_2. \end{aligned}$$

Remark 2: The lower bounds for the cosines can be obtained directly using [52, equation 12]. The proofs follow along the same lines as those of the sines given in Appendix B.

The following theorem bounds from above in the 2- and Frobenius norms the largest principal angles between the approximate and exact subspaces. This is called the *distance* between the two subspaces [14, Section 2.6.3].

Theorem 3: Under the hypotheses of Theorem 2, we have

$$\begin{aligned} \|\sin\angle(\mathcal{R}(\mathbf{Q}), \mathcal{R}(\mathbf{U}_k))\|_{2,F} &\leq \frac{\delta_k^{2q+1} \|\Phi_2 \Phi_1^\dagger\|_2 \|\Sigma_\perp\|_{2,F}}{\sigma_k \sqrt{1 + \gamma^{4q+4} \|\Phi_2 \Phi_1^\dagger\|_2^2}}, \\ \|\sin\angle(\mathcal{R}(\mathbf{P}), \mathcal{R}(\mathbf{V}_k))\|_{2,F} &\leq \frac{\delta_k^{2q} \|\Phi_2 \Phi_1^\dagger\|_2 \|\Sigma_\perp\|_{2,F}}{\sigma_k \sqrt{1 + \gamma^{4q+2} \|\Phi_2 \Phi_1^\dagger\|_2^2}}. \end{aligned}$$

Proof. The proof is presented in Appendix C.

The following theorem furnishes upper bounds for the sine of principal angles between the approximate subspaces and those spanned by individual singular vectors.

Theorem 4: Under the hypotheses of Theorem 2, we have

$$\begin{aligned} \sin\angle(\mathcal{R}(\mathbf{Q}), \mathcal{R}(\mathbf{u}_i)) &\leq \frac{\delta_i^{2q+2} \|\Phi_2 \Phi_1^\dagger\|_2}{\sqrt{1 + \gamma^{4q+4} \|\Phi_2 \Phi_1^\dagger\|_2^2}}, \\ \sin\angle(\mathcal{R}(\mathbf{P}), \mathcal{R}(\mathbf{v}_i)) &\leq \frac{\delta_i^{2q+1} \|\Phi_2 \Phi_1^\dagger\|_2}{\sqrt{1 + \gamma^{4q+2} \|\Phi_2 \Phi_1^\dagger\|_2^2}}. \end{aligned}$$

Proof. The proof is presented in Appendix D.

Theorem 4 states that $\theta_i \leq \angle(\mathcal{R}(\mathbf{Q}), \mathcal{R}(\mathbf{u}_i))$ and $\phi_i \leq \angle(\mathcal{R}(\mathbf{P}), \mathcal{R}(\mathbf{v}_i))$. This is because $\mathbf{u}_i \subseteq \mathbf{U}_k$ and $\mathbf{v}_i \subseteq \mathbf{V}_k$.

C. Bounds for Low-Rank Approximation Errors

When the left or right singular vectors are used to construct the low-rank approximation of a matrix through orthogonal projection, the error incurred remains the same. This is due to optimality of the SVD. However, unlike the SVD, the quality of approximation by RU-QLP differs when the bases in \mathbf{Q} and \mathbf{P} are used. The following theorem demonstrates this in 2- and Frobenius norms.

Theorem 5: Let \mathbf{A} be an $m \times n$ matrix whose SVD is defined in (1). Let \mathbf{A} have a RU-QLP decomposition as described in Section III, and $[\mathbf{Q}^T \mathbf{A}]_k$ and $[\mathbf{A}\mathbf{P}]_k$ be the rank- k approximations provided by the SVD. We then have

$$\begin{aligned} \|\mathbf{A} - \mathbf{Q}\mathbf{Q}^T \mathbf{A}\|_{2,F} &\leq \|\mathbf{A} - \mathbf{Q}[\mathbf{Q}^T \mathbf{A}]_k\|_{2,F} \\ &\leq \left(1 + \frac{\delta_k^{2q+1} \|\Phi_2 \Phi_1^\dagger\|_2}{1 + \gamma^{4q+4} \|\Phi_2 \Phi_1^\dagger\|_2^2}\right) \|\Sigma_\perp\|_{2,F}. \end{aligned}$$

$$\begin{aligned} \|\mathbf{A} - \mathbf{A}\mathbf{P}\mathbf{P}^T\|_{2,F} &\leq \|\mathbf{A} - [\mathbf{A}\mathbf{P}]_k \mathbf{P}^T\|_{2,F} \\ &\leq \left(1 + \frac{\delta_k^{2q} \|\Phi_2 \Phi_1^\dagger\|_2}{1 + \gamma^{4q+2} \|\Phi_2 \Phi_1^\dagger\|_2^2}\right) \|\Sigma_\perp\|_{2,F}. \end{aligned}$$

Proof. The proof is presented in Appendix E.

The first error bound of Theorem 5 is tighter than the second. This is expected and the interpretation is similar to that of principal angles θ_i and ϕ_i : since the computation of \mathbf{Q} requires \mathbf{P} , one more step of iteration is therefore needed to form \mathbf{Q} , which in turn improves its approximation quality.

D. Probabilistic Bounds

This section provides the average case analysis of RU-QLP. The random matrix used Φ is standard Gaussian. Due to rotational invariance, Φ_1 and Φ_2 have the standard normal distribution and are statistically independent.

Theorem 6: Under the hypotheses of Theorem 1, we have

$$\mathbb{E}(\sigma_k(\mathbf{R}_{11})) \geq \frac{\sigma_k}{\sqrt{1 + \delta_k^{4q+4} \omega^2}}, \quad (11)$$

$$\mathbb{E}\|\mathbf{R}_{22}\|_{2,F} \leq (1 + C\delta_k^{2q+1}) \|\Sigma_\perp\|_{2,F}, \quad (12)$$

where $\omega = \omega_1 \omega_2$, with $\omega_1 = \sqrt{m-k} + \sqrt{k+p} + 7$, $\omega_2 = \frac{4e\sqrt{k+p}}{p+1}$, and $C = \sqrt{\frac{k}{p-1} + \frac{e\sqrt{m(p+k)}}{p}}$.

Proof. The proof is given in Appendix F.

Theorem 7: Under the hypotheses of Theorem 2, we have

$$\mathbb{E}\sin\theta_i \leq \frac{\delta_i^{2q+2} \omega}{\sqrt{1 + \delta_i^{4q+4} \omega^2}}, \text{ and } \mathbb{E}\sin\phi_i \leq \frac{\delta_i^{2q+1} \omega}{\sqrt{1 + \delta_i^{4q+2} \omega^2}},$$

where ω is defined in Theorem 6.

Proof. The proof is presented in Appendix G.

Theorem 8: Under the hypotheses of Theorem 2, we have

$$\begin{aligned} \mathbb{E}\|\sin\angle(\mathcal{R}(\mathbf{Q}), \mathcal{R}(\mathbf{U}_k))\|_{2,F} &\leq \frac{\delta_k^{2q+1} \omega \|\Sigma_\perp\|_{2,F}}{\sigma_k \sqrt{1 + \delta_k^{4q+4} \omega^2}}, \\ \mathbb{E}\|\sin\angle(\mathcal{R}(\mathbf{P}), \mathcal{R}(\mathbf{V}_k))\|_{2,F} &\leq \frac{\delta_k^{2q} \omega \|\Sigma_\perp\|_{2,F}}{\sigma_k \sqrt{1 + \delta_k^{4q+2} \omega^2}}, \end{aligned}$$

where ω is defined in Theorem 6.

Theorem 9: Under the hypotheses of Theorem 2, we have

$$\begin{aligned} \mathbb{E}\sin\angle(\mathcal{R}(\mathbf{Q}), \mathcal{R}(\mathbf{u}_i)) &\leq \frac{\delta_i^{2q+2} \omega}{\sqrt{1 + \gamma^{4q+4} \omega^2}}, \\ \mathbb{E}\sin\angle(\mathcal{R}(\mathbf{P}), \mathcal{R}(\mathbf{v}_i)) &\leq \frac{\delta_i^{2q+1} \omega}{\sqrt{1 + \gamma^{4q+2} \omega^2}}, \end{aligned}$$

where ω is defined in Theorem 6.

Theorems 8 and 9 follow similarly as Theorem 7.

Theorem 10: Under the hypotheses of Theorem 5, we have

$$\mathbb{E}\|\mathbf{A} - \mathbf{Q}\mathbf{Q}^T \mathbf{A}\|_{2,F} \leq (1 + C\delta_k^{2q+1}) \|\Sigma_\perp\|_{2,F} \quad (13)$$

$$\mathbb{E}\|\mathbf{A} - \mathbf{A}\mathbf{P}\mathbf{P}^T\|_{2,F} \leq (1 + C\delta_k^{2q}) \|\Sigma_\perp\|_{2,F}, \quad (14)$$

where C is defined in Theorem 6.

The proof of this theorem is similar to that of (12).

V. NUMERICAL SIMULATIONS

This section shows the performance of RU-QLP in relation to that of several existing methods in runtime as well as the results of an empirical evaluation of the derived bounds. The simulations were performed in Python on an Intel Xeon Gold 6240 processor running at 2.6 GHz, with 18 cores and 251 GB of memory, equipped with a NVIDIA GeForce RTX 2080Ti GPU. We should add that a comprehensive comparison of RU-QLP with the state-of-the-art methods in approximation quality have been presented in [21, Section V], showing the high accuracy of RU-QLP on various classes of matrices. Hence we shall not conduct a similar study here.

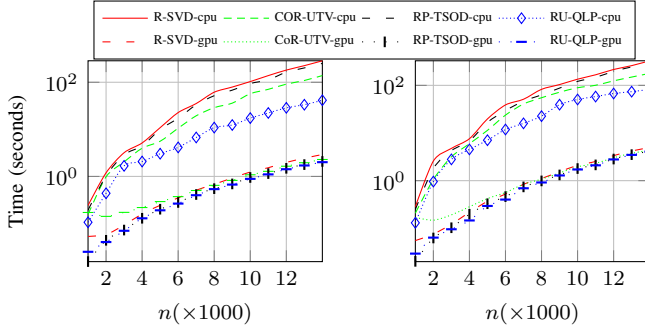


Fig. 1: Computational time for $d = 0.04n$. Left: $q = 0$. Right: $q = 2$.

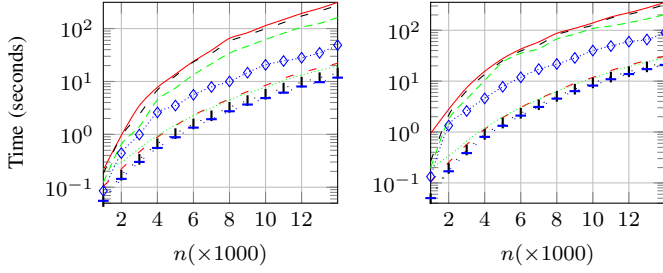


Fig. 2: Computational time for $d = 0.2n$. Left: $q = 0$. Right: $q = 2$.

A. Runtime Comparison

We generate dense $n \times n$ matrices, and use several randomized methods to factorize the matrices into three components. We consider R-SVD (randomized SVD) [20], CoR-UTV (compressed randomized UTV) [23], RP-TSOD (randomized pivoted two-sided orthogonal decomposition) [26], and RU-QLP. For the sampling size parameter d (i.e., the dimension of the reduced matrix), we consider three cases: $d = 0.04n$, $d = 0.2n$ and $d = 0.3n$. The results averaged over 10 trials are shown in Figs. 1–3. Furthermore, Figs. 4–6 show the speedups offered by RU-QLP. We make several observations:

- On the CPU, RU-QLP is substantially faster than other methods, achieving speedups of up to 7.1 times, 3.6 times, and 6.5 times over R-SVD, CoR-UTV, and RP-TSOD, respectively. The discrepancy is pronounced particularly when $q = 0$ (no power iteration case). This is because for $q \geq 1$, the cost is dominated by matrix-matrix multiplications; see Section III-B. In addition, as the size of the input matrix and the parameter d increase, RU-QLP confers more advantage.
- On the CPU-GPU architecture, in spite of the reduced gaps in computational time, RU-QLP still outperforms other methods, achieving speedups of up to 2.3 times, 6.8 times, and 1.5 times over R-SVD, CoR-UTV, and RP-TSOD, respectively. Moreover, by increasing the size of the input matrix and particularly d , RU-QLP starts to become more efficient.
- RU-QLP is faster than CoR-UTV, RP-TSOD and R-SVD, because it only makes use of unpivoted QR, which leverages the parallel structure of modern machines better than pivoted QR and the SVD employed in other methods. CoR-UTV and RP-TSOD are more efficient than R-SVD,

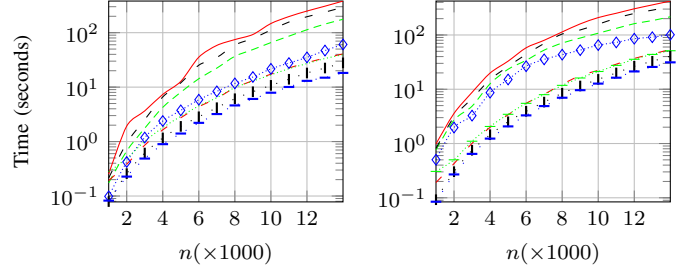


Fig. 3: Computational time for $d = 0.3n$. Left: $q = 0$. Right: $q = 2$.

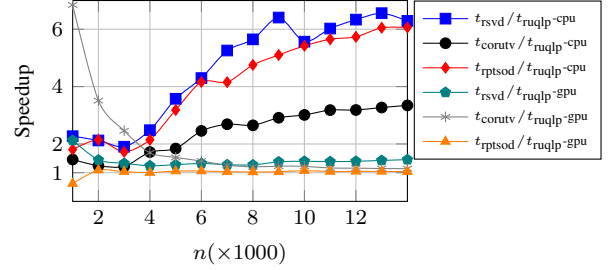


Fig. 4: Speedup for $d = 0.04n$ with $q = 0$.

because they utilize pivoted QR, which imposes less communication cost than the SVD; see Section II-C2.

B. Evaluation of Error Bounds

We construct four $n \times n$ matrices, and consider one from an application. The first two matrices have the following form:

$$\mathbf{A} = \mathbf{U}\mathbf{\Sigma}\mathbf{V}^T + \mu\sigma_k\mathbf{A}_N, \quad (15)$$

where \mathbf{U} and \mathbf{V} are random orthogonal matrices, and $\mathbf{\Sigma}$ is diagonal with elements σ_i s decreasing linearly from 1 to 10^{-10} , and $\sigma_{i+1} = 0$ for $i \geq k$. and \mathbf{A}_N is a normalized Gaussian matrix. Two cases for μ are considered: i) $\mu = 0.005$, giving the matrix `LowRankLargeGap`; and ii) $\mu = 0.01$, giving the matrix `LowRankMediumGap`.

The second two matrices take the form $\mathbf{A} = \mathbf{U}\mathbf{\Sigma}\mathbf{V}^T$, with

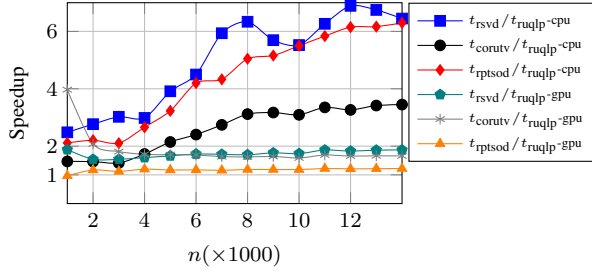
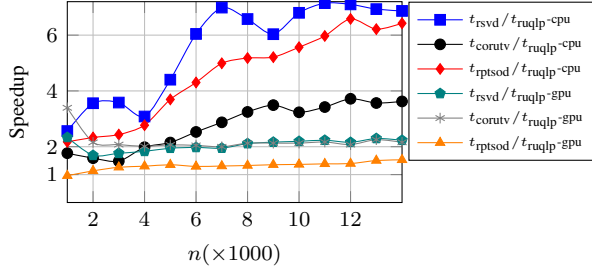
$$\mathbf{\Sigma} = \text{diag}(\underbrace{1, \dots, 1}_k, 2^{-z}, 3^{-z}, \dots, (n-k+1)^{-z}). \quad (16)$$

Two cases for p are considered: i) $z = 1$, giving the matrix `LowRankSlowDecay`; and ii) $z = 2$, giving the matrix `LowRankFastDecay`. These matrices were used in [42]. We set for the four matrices $n = 800$, $k = 16$, and $p = 16$, hence $d = 32$.

The fifth matrix `impcol_e` is from a hydrocarbon separation problem taken from SuiteSparse Matrix Collection [54]. This matrix is of order 225 and has a well-defined gap between σ_{10} and σ_{11} .

The singular values of the matrices with their estimations by RU-QLP are displayed in Figs. 7–9. They show clearly the rank-revealing property and high accuracy of RU-QLP.

1) *Principal angles*: We compute the sines of principal angles, $\sin\theta_i$ and $\sin\phi_i$, between left and right approximate subspaces and the corresponding singular subspaces, and compare them to the theoretical upper bounds given in Theorem

Fig. 5: Speedup for $d = 0.2n$ with $q = 0$.Fig. 6: Speedup for $d = 0.3n$ with $q = 0$.

2. The results are shown in Figs. 10–14. We make several observations: i) if there is a well-defined gap in the spectrum, the bounds are qualitatively accurate. Also, the bounds become more accurate as the gap gets larger; ii) The bounds are quantitatively informative for polynomially decaying spectrums. The principal angles become smaller as the spectrum decays faster. iii) As the power factor q increases, the angles become smaller, and hence the approximate subspaces become more accurate; iv) θ_i are smaller than ϕ_i , or \mathbf{Q} is a better approximation to \mathbf{U}_k than \mathbf{P} is to \mathbf{V}_k , due to the construction of these matrices by RU-QLP (see the explanation in Theorem 2).

2) *Low-rank approximation*: We compute approximation errors in both spectral and Frobenius norms incurred by RU-QLP through forming the orthogonal projections by \mathbf{Q} and \mathbf{P} . We compare the errors to the theoretical upper bounds furnished in Theorem 5 and to those incurred by the optimal SVD. The results are shown in Figs. 15–24. We make several observations: i) when the power factor $q = 0$, the bounds are qualitatively informative, particularly for the spectral norm cases; ii) when $q \geq 1$, the effect on the theoretical bounds is pronounced, as they become qualitatively tight in most cases; iii) for $q = 2$, the approximation errors closely match those of the optimal SVD in all cases, showing high quality of approximate left and right subspaces.

VI. CONCLUSION

In this paper, we presented the rank-revealing RU-QLP decomposition, which furnishes an approximation to the SVD and pivoted QLP. We presented a new error analysis, developing bounds on the rank-revealing property, principal angles between approximate subspaces and exact singular subspaces and vectors, and on the low-rank approximation errors. We investigated the accuracy of the bounds on five matrices. We further investigated the runtime performance of RU-QLP and

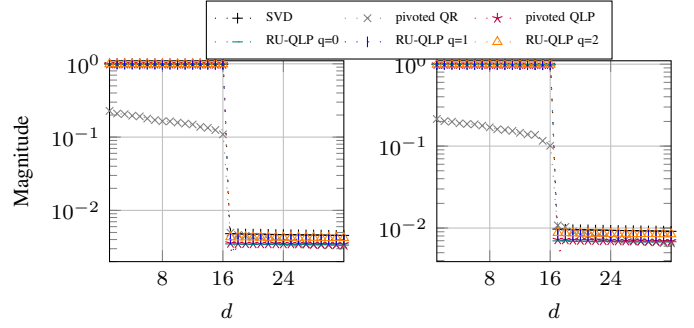


Fig. 7: Singular values of LowRankLargeGap (left), LowRankMediumGap (right)

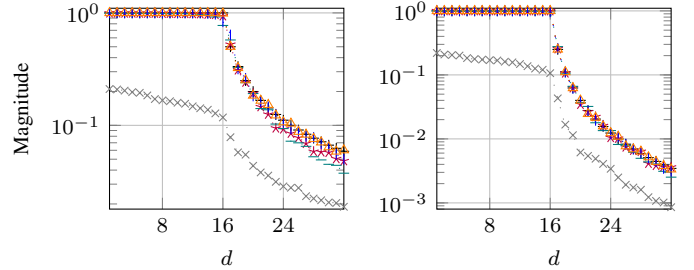


Fig. 8: Singular values of LowRankSlowDecay (left), LowRankFastDecay (right).

several existing methods on a multicore computer equipped with a GPU. Our results showed that RU-QLP harnesses best the modern computing architectures and can be viewed as the fastest randomized method in the literature.

APPENDIX A PROOF OF THEOREM 1

Remark 3: Before proving our results, we should add that we use the SVD partitioning of the matrix \mathbf{A} as in (1), a 2×2 block $\mathbf{\Sigma}$ and 2×1 blocks \mathbf{U} and \mathbf{V} . It is however possible to use a 3×3 block for $\mathbf{\Sigma}$ and 3×1 blocks for the orthogonal matrices to derive more bounds on the principal angles between subspaces based on the CS decomposition [55]. This is particularly useful when the SVD is used to construct the low-rank factorization; see [56], [57].

By the Cauchy interlacing theorem [58, Theorem 4.3.17], we have

$$\begin{aligned} \lambda_i(\mathbf{A}^T \mathbf{A}) &\geq \lambda_i(\mathbf{R}^T \mathbf{R}) \geq \lambda_i(\mathbf{R}_{11}^T \mathbf{R}_{11}) \\ &= \lambda_i(\bar{\mathbf{P}}_1^T \mathbf{A}^T \mathbf{Q}_1 \mathbf{Q}_1^T \mathbf{A} \bar{\mathbf{P}}_1), \end{aligned}$$

where the last relation is due to the first equality in (5). We now compute $\mathbf{Q}_1 \mathbf{Q}_1^T$. We have for the range of \mathbf{Q} :

$$\mathcal{R}(\mathbf{Q}) = \mathcal{R}(\mathbf{A} \bar{\mathbf{P}}) = \mathcal{R}(\mathbf{A}(\mathbf{A}^T \mathbf{A})^q \mathbf{A}^T \Phi).$$

We define a non-singular $d \times d$ matrix $\mathbf{Y} \triangleq [\Phi_1^\dagger \Sigma_k^{-(2q+2)} \bar{\mathbf{Y}}]$ such that $\Phi_1 \bar{\mathbf{Y}} = \mathbf{0}$. We assume that the rank of Φ_1 is k such that $\Phi_1 \Phi_1^\dagger = \mathbf{I}$. We then form the following matrix product and compute its QR factorization:

$$\begin{aligned} \mathbf{A}(\mathbf{A}^T \mathbf{A})^q \mathbf{A}^T \Phi \mathbf{Y} &= \mathbf{U} \begin{bmatrix} \mathbf{I} & \mathbf{0} \\ \mathbf{S} & \Sigma_{11}^{2q+2} \Phi_2 \bar{\mathbf{Y}} \end{bmatrix} = \dot{\mathbf{Q}} \dot{\mathbf{R}} \\ &= [\dot{\mathbf{Q}}_1 \quad \dot{\mathbf{Q}}_2] \begin{bmatrix} \dot{\mathbf{R}}_{11} & \dot{\mathbf{R}}_{12} \\ \mathbf{0} & \dot{\mathbf{R}}_{22} \end{bmatrix}, \end{aligned}$$

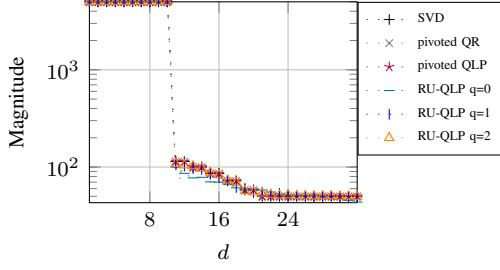
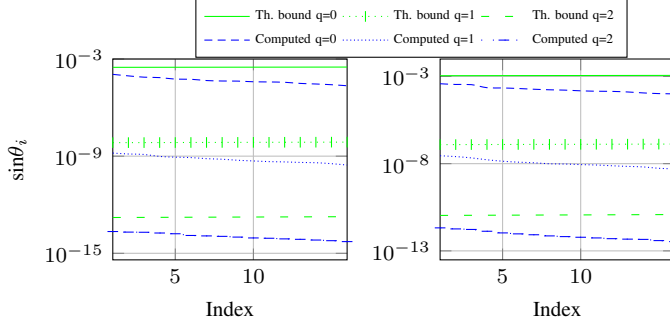


Fig. 9: Singular values of impcol_e

Fig. 10: Principal angles between $\mathcal{R}(\mathbf{Q})$ and $\mathcal{R}(\mathbf{U}_k)$ for LowRankLargeGap (left), and LowRankMediumGap (right).

where $\mathbf{S} \triangleq \Sigma_{\perp}^{2q+2} \Phi_2 \Phi_1^{\dagger} \Sigma_k^{-(2q+2)}$. Since \mathbf{Y} is non-singular, $\mathcal{R}(\mathbf{Q}) = \mathcal{R}(\dot{\mathbf{Q}})$. This means that there is an orthogonal matrix \mathbf{W} such that $\mathbf{Q} = \dot{\mathbf{Q}}\mathbf{W}$, thus giving $\mathbf{Q}\mathbf{Q}^T = \dot{\mathbf{Q}}\dot{\mathbf{Q}}^T$. From the above equation, we obtain $\mathbf{Q}_1 = \mathbf{U}[\mathbf{I}^T \quad \mathbf{S}^T]^T \mathbf{R}_{11}^{-1}$, and hence we get

$$\mathbf{Q}_1 \mathbf{Q}_1^T = \dot{\mathbf{Q}}_1 \dot{\mathbf{Q}}_1^T = \mathbf{U} \begin{bmatrix} \bar{\mathbf{S}} & \bar{\mathbf{S}}\mathbf{S}^T \\ \bar{\mathbf{S}}\mathbf{S} & \bar{\mathbf{S}}\mathbf{S}\mathbf{S}^T \end{bmatrix} \mathbf{U}^T, \quad (17)$$

where $\bar{\mathbf{S}}$ is defined as follows:

$$\bar{\mathbf{S}} \triangleq \mathbf{R}_{11}^{-1} \dot{\mathbf{R}}_{11}^{-T} = (\mathbf{R}_{11}^T \dot{\mathbf{R}}_{11})^{-1} = (\mathbf{I} + \mathbf{S}^T \mathbf{S})^{-1}. \quad (18)$$

We now form $\bar{\mathbf{P}}_1^T \mathbf{A}^T \mathbf{Q}_1 \mathbf{Q}_1^T \mathbf{A} \bar{\mathbf{P}}_1$

$$\begin{aligned} & \bar{\mathbf{P}}_1^T \mathbf{A}^T \mathbf{Q}_1 \mathbf{Q}_1^T \mathbf{A} \bar{\mathbf{P}}_1 = \\ & \bar{\mathbf{P}}_1^T \mathbf{V} \begin{bmatrix} \Sigma_k \bar{\mathbf{S}} \Sigma_k & \Sigma_k \bar{\mathbf{S}} \mathbf{S}^T \Sigma_{\perp} \\ \Sigma_{\perp} \bar{\mathbf{S}} \mathbf{S} \Sigma_k & \Sigma_{\perp} \bar{\mathbf{S}} \mathbf{S} \mathbf{S}^T \Sigma_{\perp} \end{bmatrix} \mathbf{V}^T \bar{\mathbf{P}}_1. \end{aligned}$$

Since $\Sigma_k \bar{\mathbf{S}} \Sigma_k$ is a submatrix, we have for $i = 1, \dots, k$

$$\lambda_i(\bar{\mathbf{P}}_1^T \mathbf{A}^T \mathbf{Q}_1 \mathbf{Q}_1^T \mathbf{A} \bar{\mathbf{P}}_1) \geq \lambda_i(\Sigma_k \bar{\mathbf{S}} \Sigma_k). \quad (19)$$

Due to matrix partial orderings [58, Section 7.7], it follows

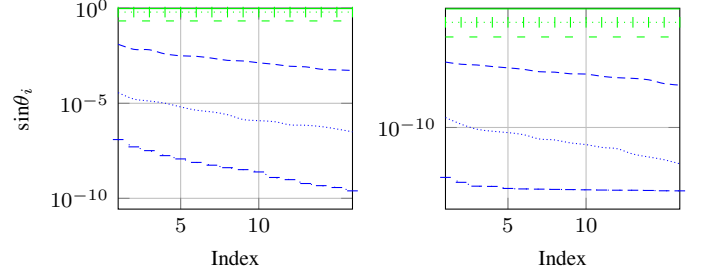
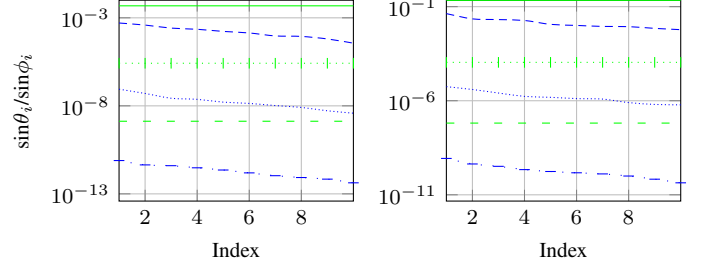
$$\mathbf{S}^T \mathbf{S} \preceq \sigma_{k+1}^{4q+4} \|\Phi_2 \Phi_1^{\dagger}\|_2^2 \Sigma_k^{-(4q+4)} = \Delta^{(4q+4)} \|\Phi_2 \Phi_1^{\dagger}\|_2^2, \quad (20)$$

where $\Delta = \text{diag}(\delta_1, \dots, \delta_k)$ is a $k \times k$ matrix with entries $\delta_i = \frac{\sigma_{k+1}}{\sigma_i}$. Accordingly, we have

$$\Sigma_k (\mathbf{I} + \mathbf{S}^T \mathbf{S})^{-1} \Sigma_k \succeq \Sigma_k (\mathbf{I} + \Delta^{(4q+4)} \|\Phi_2 \Phi_1^{\dagger}\|_2^2)^{-1} \Sigma_k,$$

which results in

$$\begin{aligned} \lambda_i(\mathbf{A}^T \mathbf{A}) & \geq \lambda_i(\mathbf{R}_{11}^T \mathbf{R}_{11}) \geq \lambda_i(\Sigma_k (\mathbf{I} + \mathbf{S}^T \mathbf{S})^{-1} \Sigma_k) \\ & \geq \frac{\sigma_i^2}{1 + \delta_i^{4q+4} \|\Phi_2 \Phi_1^{\dagger}\|_2^2}. \end{aligned}$$

Fig. 11: Principal angles between $\mathcal{R}(\mathbf{Q})$ and $\mathcal{R}(\mathbf{U}_k)$ for LowRankSlowDecay (left), and LowRankFastDecay (right).Fig. 12: Principal angles between $\mathcal{R}(\mathbf{Q})$ and $\mathcal{R}(\mathbf{U}_k)$ (left) and between $\mathcal{R}(\mathbf{P})$ and $\mathcal{R}(\mathbf{V}_k)$ (right) for impcol_e.

By taking the square root of the last identity, we get the bounds for the first k singular values of \mathbf{R}_{11} .

To prove (8), we get from the second equality in (6)

$$\begin{aligned} \|\mathbf{R}_{22}\|_{2,F} & = \|\mathbf{Q}_2^T \mathbf{A} \bar{\mathbf{P}}_2\|_{2,F} = \|\mathbf{Q}_2 \mathbf{Q}_2^T \mathbf{A} \bar{\mathbf{P}}_2\|_{2,F} \\ & \leq \|(\mathbf{I} - \mathbf{Q}_1 \mathbf{Q}_1^T) \mathbf{A}\|_{2,F} \leq \|(\mathbf{I} - \mathbf{Q}_1 \mathbf{Q}_1^T) \mathbf{A}_k\|_{2,F} + \|\mathbf{A}_{\perp}\|_{2,F}. \end{aligned} \quad (21)$$

The second equality is due to the unitary invariance of the 2- and Frobenius norms, the first inequality follows because $\bar{\mathbf{P}}_2$ has orthonormal columns, and the second inequality is due to the triangle inequality after writing $\mathbf{A} = \mathbf{A}_k + \mathbf{A}_{\perp}$. To bound $\|(\mathbf{I} - \mathbf{Q}_1 \mathbf{Q}_1^T) \mathbf{A}_k\|_{2,F}$ from above, we write $\mathbf{A}_k = \mathbf{U}[\Sigma_k \quad \mathbf{0}; \mathbf{0} \quad \mathbf{0}] \mathbf{V}^T$, which, together with (17), gives

$$(\mathbf{I} - \mathbf{Q}_1 \mathbf{Q}_1^T) \mathbf{A}_k = \mathbf{U} \begin{bmatrix} (\mathbf{I} - \bar{\mathbf{S}}) \Sigma_k \\ -\bar{\mathbf{S}} \mathbf{S} \Sigma_k \end{bmatrix} \mathbf{V}^T.$$

It follows that

$$\begin{aligned} \|(\mathbf{I} - \mathbf{Q}_1 \mathbf{Q}_1^T) \mathbf{A}_k\|_{2,F}^2 & = \|\Sigma_k (\mathbf{I} - \bar{\mathbf{S}}) \Sigma_k\|_{2,F}^2 \\ & = \|\Sigma_k \mathbf{S}^T (\mathbf{I} + \mathbf{S} \mathbf{S}^T)^{-1} \Sigma_k\|_{2,F}^2 = \|\Sigma_k^{-(2q+1)} (\Phi_2 \Phi_1^{\dagger})^T \\ & \times \Sigma_{\perp}^{2q+2} (\mathbf{I} + \mathbf{S} \mathbf{S}^T)^{-1} \Sigma_{\perp}^{2q+2} \Phi_2 \Phi_1^{\dagger} \Sigma_k^{-(2q+1)}\|_{2,F}^2 \\ & \leq \delta_k^{4q+2} \|\Phi_2 \Phi_1^{\dagger}\|_2^2 \|(\mathbf{I} + \mathbf{S} \mathbf{S}^T)^{-1}\|_2^2 \|\Sigma_{\perp}\|_{2,F}^2. \end{aligned}$$

The second equality is due to the Sherman–Morrison–Woodbury formula [58, Section 0.7.4], and the last relation follows from the strong submultiplicativity property for the Frobenius norm [59, equation 9.3.13] holding for any matrices \mathbf{A} and \mathbf{B} with appropriate dimensions:

$$\begin{aligned} \|\mathbf{A}\mathbf{B}\|_F & \leq \|\mathbf{A}\|_F \sigma_1(\mathbf{B}), \\ \|\mathbf{A}\mathbf{B}\|_F & \leq \sigma_1(\mathbf{A}) \|\mathbf{B}\|_F. \end{aligned} \quad (22)$$

The non-zero eigenvalues of $(\mathbf{I} + \mathbf{S} \mathbf{S}^T)^{-1}$ are:

$$1/1 + \sigma_i^2(\mathbf{S}). \quad (23)$$

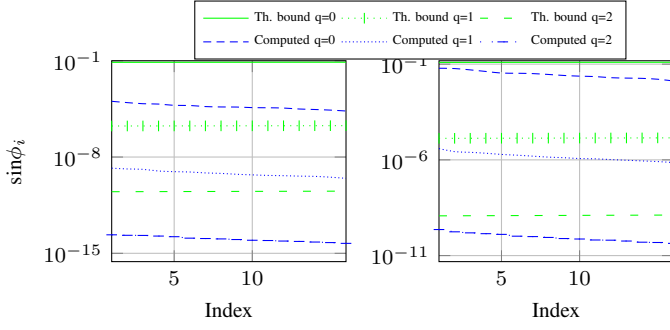


Fig. 13: Principal angles between $\mathcal{R}(\mathbf{P})$ and $\mathcal{R}(\mathbf{V}_k)$ for LowRankLargeGap (left), and LowRankMediumGap (right).

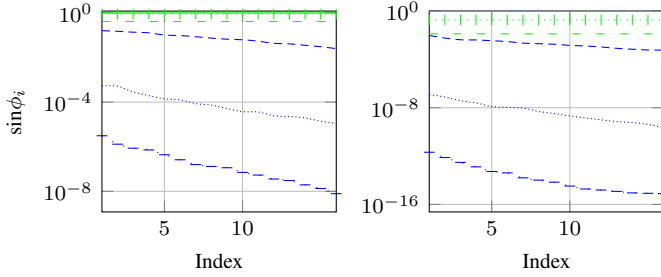


Fig. 14: Principal angles between $\mathcal{R}(\mathbf{P})$ and $\mathcal{R}(\mathbf{V}_k)$ for LowRankSlowDecay (left), and LowRankFastDecay (right).

$\sigma_1(\mathbf{S})$ is bounded from below by:

$$\sigma_1(\mathbf{S}) \geq \gamma^{2q+2} \|\Phi_2 \Phi_1^\dagger\|_2, \quad (24)$$

where $\gamma = \sigma_n/\sigma_1$, and we have used the following relations [60, p. 80] that hold for any unitary invariant norm:

$$\begin{aligned} \|\mathbf{AB}\| &\geq \|\mathbf{A}\| \sigma_{\min}(\mathbf{B}), \\ \|\mathbf{AB}\| &\geq \sigma_{\min}(\mathbf{A}) \|\mathbf{B}\|. \end{aligned}$$

Thus

$$\|(\mathbf{I} + \mathbf{SS}^T)^{-1}\|_2 \leq \frac{1}{1 + \gamma^{4q+4} \|\Phi_2 \Phi_1^\dagger\|_2^2}. \quad (25)$$

Upon substitution and taking the square root, we obtain

$$\|(\mathbf{I} - \mathbf{Q}_1 \mathbf{Q}_1^T) \mathbf{A}_k\|_{2,F} \leq \frac{\delta_k^{2q+1} \|\Phi_2 \Phi_1^\dagger\|_2}{1 + \gamma^{4q+4} \|\Phi_2 \Phi_1^\dagger\|_2^2} \|\Sigma_\perp\|_{2,F}, \quad (26)$$

Inserting this bound into (21) gives the desired result. \square

APPENDIX B PROOF OF THEOREM 2

We make use of a result from [52, equation 13], which states in our notation that the SVD of the matrix product $(\mathbf{I} - \mathbf{P}_Q) \mathbf{U}_k$ gives the sines of canonical angles between the two subspaces spanned by \mathbf{Q} and \mathbf{U}_k . In particular, let

$$(\mathbf{I} - \mathbf{P}_Q) \mathbf{U}_k = \mathbf{Y}_Q \mathbf{S}_Q \mathbf{Z}_Q^T,$$

then, the matrix $\mathbf{S}_Q \in \mathbb{R}^{k \times k}$ contains on the diagonal the sines of canonical angles $\sin \theta_i$. Further

$$\begin{aligned} \mathbf{U}_k^T (\mathbf{I} - \mathbf{P}_Q) \mathbf{U}_k &= \mathbf{Z}_Q^T \mathbf{S}_Q^2 \mathbf{Z}_Q = \mathbf{U}_k^T (\mathbf{I} - \mathbf{P}_Q) \mathbf{U}_k \\ &\preceq \mathbf{U}_k^T (\mathbf{I} - \mathbf{P}_{Q_1}) \mathbf{U}_k. \end{aligned}$$

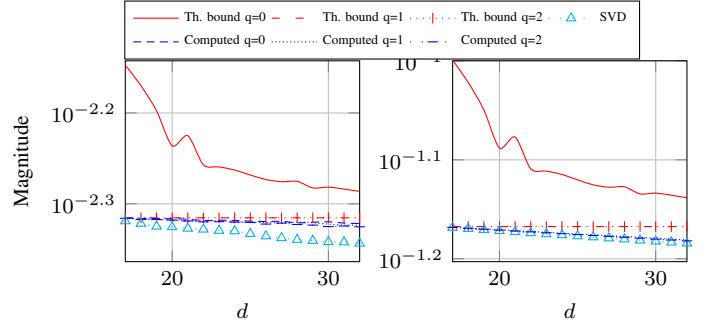


Fig. 15: \mathbf{Q} -based low-rank approximation error for LowRankLargeGap. Left: Spectral norm. Right: Frobenius norm.

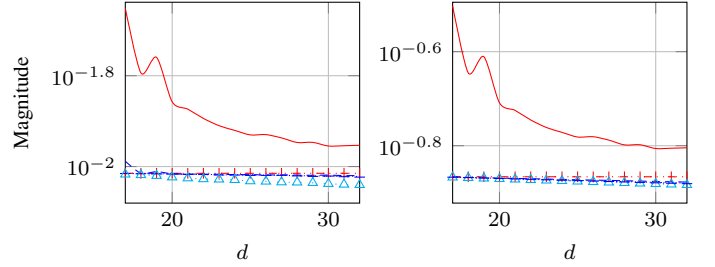


Fig. 16: \mathbf{Q} -based low-rank approximation error for LowRankMediumGap. Left: Spectral norm. Right: Frobenius norm.

The last relation holds because $\dot{\mathbf{Q}}_1$ contains k columns of $\dot{\mathbf{Q}}$. Upon substitution, we get

$$\mathbf{U}_k^T (\mathbf{I} - \mathbf{P}_{\dot{\mathbf{Q}}_1}) \mathbf{U}_k = \begin{bmatrix} \mathbf{I} & \mathbf{0} \\ -\mathbf{S}\bar{\mathbf{S}} & \mathbf{I} - \mathbf{S}\bar{\mathbf{S}}\mathbf{S}^T \end{bmatrix} \begin{bmatrix} \mathbf{I} \\ \mathbf{0} \end{bmatrix} = \mathbf{I} - \bar{\mathbf{S}}.$$

The matrix $\mathbf{I} - \bar{\mathbf{S}} = \mathbf{S}^T \mathbf{S} (\mathbf{I} + \mathbf{S}^T \mathbf{S})^{-1}$ is positive semidefinite, and its eigenvalues satisfy [60, p. 148]:

$$\lambda_i(\mathbf{I} - \bar{\mathbf{S}}) = \frac{\sigma_i^2(\mathbf{S})}{1 + \sigma_i^2(\mathbf{S})}, \quad i = 1, \dots, k.$$

We obtain for the singular values of \mathbf{S}

$$\sigma_i(\mathbf{S}) \leq \sigma_1(\Sigma_\perp^{2q+2} \Phi_2 \Phi_1^\dagger) \sigma_i(\Sigma_k^{-(2q+2)}) \leq \frac{\sigma_{k+1}^{2q+2}}{\sigma_{k-i+1}^{2q+2}} \|\Phi_2 \Phi_1^\dagger\|_2,$$

where we have used [59, equation 9.6.2]

$$\sigma_i(\mathbf{AB}) = \sigma_i(\mathbf{A}) \sigma_i(\mathbf{B}). \quad (27)$$

Since $\mathbf{Z}_Q \mathbf{S}_Q^2 \mathbf{Z}_Q^T \preceq \mathbf{I} - \bar{\mathbf{S}}$, the Weyl's inequality [59, Theorem 8.4.9] implies that

$$\sin^2 \theta_i \leq \lambda_i(\mathbf{I} - \bar{\mathbf{S}}). \quad (28)$$

Upon substitution, taking the square root, and renaming $i \leftarrow k - i + 1$, the result in (9) follows.

The proof of (10) is similar to that of (9). We first have

$$(\mathbf{I} - \mathbf{P}_P) \mathbf{V}_k = \mathbf{Y}_P \mathbf{S}_P \mathbf{Z}_P^T, \quad (29)$$

where the matrix $\mathbf{S}_P \in \mathbb{R}^{k \times k}$ contains on the diagonal the sines of canonical angles $\sin \phi_i$ between the two subspaces spanned by \mathbf{P} and \mathbf{V}_k . We now compute \mathbf{P}_P . Since $\bar{\mathbf{P}}$ is an orthogonal matrix, we have for the range of \mathbf{P} :

$$\mathcal{R}(\mathbf{P}) = \mathcal{R}(\bar{\mathbf{P}}) = \mathcal{R}((\mathbf{A}^T \mathbf{A})^q \mathbf{A}^T \Phi).$$

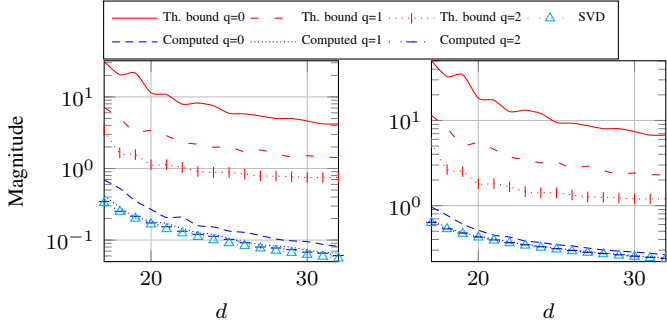


Fig. 17: **Q**-based low-rank approximation error for LowRankSlowDecay. Left: Spectral norm. Right: Frobenius norm.

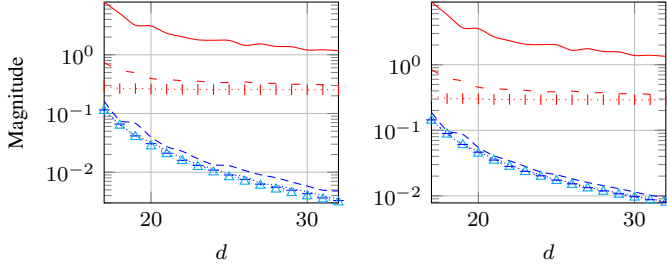


Fig. 18: **Q**-based low-rank approximation error for LowRankFastDecay. Left: Spectral norm. Right: Frobenius norm.

We define a non-singular $d \times d$ matrix $\mathbf{X} \triangleq [\Phi_1^\dagger \Sigma_k^{-(2q+1)} \bar{\mathbf{X}}]$ such that $\Phi_1 \mathbf{X} = \mathbf{0}$. We form the following matrix product and compute its QR factorization:

$$\begin{aligned} (\mathbf{A}^T \mathbf{A})^q \mathbf{A}^T \Phi \mathbf{X} &= \mathbf{V} \begin{bmatrix} \mathbf{I} & \mathbf{0} \\ \mathbf{J} & \Sigma_{\perp}^{2q+1} \Phi_2 \bar{\mathbf{X}} \end{bmatrix} = \bar{\mathbf{Q}} \bar{\mathbf{R}} \\ &= [\bar{\mathbf{Q}}_1 \quad \bar{\mathbf{Q}}_2] \begin{bmatrix} \bar{\mathbf{R}}_{11} & \bar{\mathbf{R}}_{12} \\ \mathbf{0} & \bar{\mathbf{R}}_{22} \end{bmatrix}, \end{aligned}$$

where $\mathbf{J} \triangleq \Sigma_{\perp}^{2q+1} \Phi_2 \Phi_1^\dagger \Sigma_k^{-(2q+1)}$. Since \mathbf{X} is non-singular, $\mathcal{R}(\bar{\mathbf{P}}) = \mathcal{R}(\bar{\mathbf{Q}})$. This means that there is an orthogonal matrix \mathbf{W} such that $\bar{\mathbf{P}} = \bar{\mathbf{Q}} \mathbf{W}$, thus giving $\bar{\mathbf{P}} \bar{\mathbf{P}}^T = \bar{\mathbf{Q}} \bar{\mathbf{Q}}^T$. From the above equation, we have $\bar{\mathbf{Q}}_1 = \mathbf{V} [\mathbf{I}^T \quad \mathbf{J}^T]^T \bar{\mathbf{R}}_{11}^{-1}$, and hence obtain for $\bar{\mathbf{P}}_1 \bar{\mathbf{P}}_1^T$

$$\bar{\mathbf{P}}_1 \bar{\mathbf{P}}_1^T = \bar{\mathbf{Q}}_1 \bar{\mathbf{Q}}_1^T = \mathbf{V} \begin{bmatrix} \bar{\mathbf{J}} & \bar{\mathbf{J}} \bar{\mathbf{J}}^T \\ \bar{\mathbf{J}} \bar{\mathbf{J}} & \bar{\mathbf{J}} \bar{\mathbf{J}} \bar{\mathbf{J}}^T \end{bmatrix} \mathbf{V}^T,$$

where $\bar{\mathbf{J}}$ is defined as follows:

$$\bar{\mathbf{J}} \triangleq \bar{\mathbf{R}}_{11}^{-1} \bar{\mathbf{R}}_{11}^{-T} = (\bar{\mathbf{R}}_{11}^T \bar{\mathbf{R}}_{11})^{-1} = (\mathbf{I} + \mathbf{J}^T \mathbf{J})^{-1}. \quad (30)$$

Having obtained $\bar{\mathbf{P}}_P$, it follows from (29) that

$$\begin{aligned} \mathbf{V}_k^T (\mathbf{I} - \mathbf{P}_P) \mathbf{V}_k &= \mathbf{Z}_P \mathbf{S}_P^2 \mathbf{Z}_P^T = \mathbf{V}_k^T (\mathbf{I} - \mathbf{P}_{\bar{\mathbf{Q}}}) \mathbf{V}_k \\ &\leq \mathbf{V}_k^T (\mathbf{I} - \mathbf{P}_{\bar{\mathbf{Q}}_1}) \mathbf{V}_k \\ &= [\mathbf{I} \quad \mathbf{0}] \begin{bmatrix} \mathbf{I} - \bar{\mathbf{J}} & -\bar{\mathbf{J}} \bar{\mathbf{J}}^T \\ -\bar{\mathbf{J}} \bar{\mathbf{J}} & \mathbf{I} - \bar{\mathbf{J}} \bar{\mathbf{J}} \bar{\mathbf{J}}^T \end{bmatrix} \begin{bmatrix} \mathbf{I} \\ \mathbf{0} \end{bmatrix} = \mathbf{I} - \bar{\mathbf{J}}. \end{aligned}$$

The rest is similar to the proof of (9), we thus omit it. \square

APPENDIX C

PROOF OF THEOREM 3

From the proof of Theorem 2, we have

$$\mathbf{Z}_Q \mathbf{S}_Q^2 \mathbf{Z}_Q^T \preceq \mathbf{I} - \bar{\mathbf{S}} = \mathbf{S}^T \mathbf{S} (\mathbf{I} + \mathbf{S}^T \mathbf{S})^{-1},$$

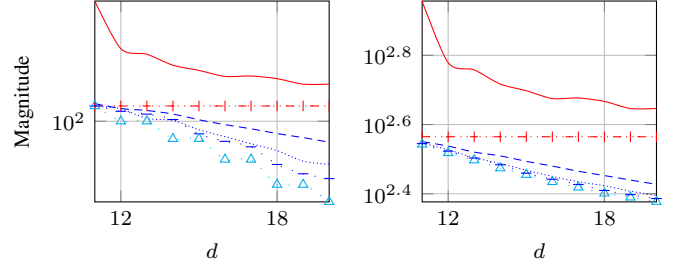


Fig. 19: **Q**-based low-rank approximation error for imprecol_e. Left: Spectral norm. Right: Frobenius norm.

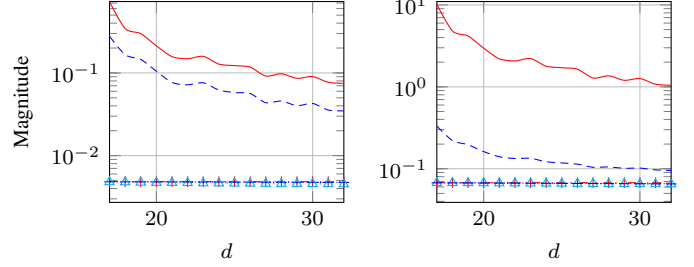


Fig. 20: **P**-based low-rank approximation error for LowRankLargeGap. Left: Spectral norm. Right: Frobenius norm.

which gives

$$\|\mathbf{Z}_U \mathbf{S}_U^2 \mathbf{Z}_U^T\|_{2,F} \leq \|\mathbf{S}^T \mathbf{S}\|_{2,F} \|(\mathbf{I} + \mathbf{S}^T \mathbf{S})^{-1}\|_2,$$

where we have used (22). Using (25) and (22), the result follows. The proof for the other bound is similar, we thus omit it. \square

APPENDIX D

PROOF OF THEOREM 4

The proof of this theorem follows that of Theorem 2. For $i = 1, \dots, k$, let \mathbf{u}_i be the i th left singular vector of \mathbf{A} . We then have

$$\begin{aligned} \sin^2 \angle(\mathcal{R}(\mathbf{Q}), \mathcal{R}(\mathbf{u}_i)) &= \mathbf{u}_i^T (\mathbf{I} - \mathbf{P}_Q) \mathbf{u}_i \leq \mathbf{u}_i^T (\mathbf{I} - \mathbf{P}_{\bar{\mathbf{Q}}_1}) \mathbf{u}_i \\ &= [\mathbf{e}_i^T \quad \mathbf{0}] \begin{bmatrix} \mathbf{I} - \bar{\mathbf{S}} & -\bar{\mathbf{S}} \bar{\mathbf{S}}^T \\ -\bar{\mathbf{S}} \bar{\mathbf{S}} & \mathbf{I} - \bar{\mathbf{S}} \bar{\mathbf{S}} \bar{\mathbf{S}}^T \end{bmatrix} \begin{bmatrix} \mathbf{e}_i \\ \mathbf{0} \end{bmatrix} \leq \mathbf{e}_i^T (\mathbf{I} - \bar{\mathbf{S}}) \mathbf{e}_i. \end{aligned}$$

Writing $\mathbf{I} - \bar{\mathbf{S}} = \mathbf{S}^T (\mathbf{I} + \mathbf{S} \mathbf{S}^T)^{-1} \mathbf{S}$, it follows

$$\begin{aligned} \sin^2 \angle(\mathcal{R}(\mathbf{Q}), \mathcal{R}(\mathbf{u}_i)) &\leq \delta_i^{4q+4} \|\Phi_2 \Phi_1^\dagger\|_2^2 \|(\mathbf{I} + \mathbf{S} \mathbf{S}^T)^{-1}\|_2^2 \\ &\leq \frac{\delta_i^{4q+4} \|\Phi_2 \Phi_1^\dagger\|_2^2}{1 + \gamma^{4q+4} \|\Phi_2 \Phi_1^\dagger\|_2^2}. \end{aligned}$$

By taking the square root the result follows. The proof for the other bound is similar, we thus omit it. \square

APPENDIX E

PROOF OF THEOREM 5

To prove the first bound, we have

$$\begin{aligned} \|\mathbf{A} - \mathbf{Q} \mathbf{Q}^T \mathbf{A}\|_{2,F} &\leq \|\mathbf{A} - \mathbf{Q} [\mathbf{Q}^T \mathbf{A}]\|_{2,F} \\ &\leq \|\mathbf{A} - \mathbf{Q}_1 \mathbf{Q}_1^T \mathbf{A}\|_{2,F} \\ &\leq \|\mathbf{A}_{\perp} - \mathbf{Q}_1 \mathbf{Q}_1^T \mathbf{A}_{\perp}\|_{2,F} + \|\mathbf{A}_k - \mathbf{Q}_1 \mathbf{Q}_1^T \mathbf{A}_k\|_{2,F} \\ &\leq \|\mathbf{A}_{\perp}\|_{2,F} + \|\mathbf{A}_k - \mathbf{Q}_1 \mathbf{Q}_1^T \mathbf{A}_k\|_{2,F}. \end{aligned} \quad (31)$$

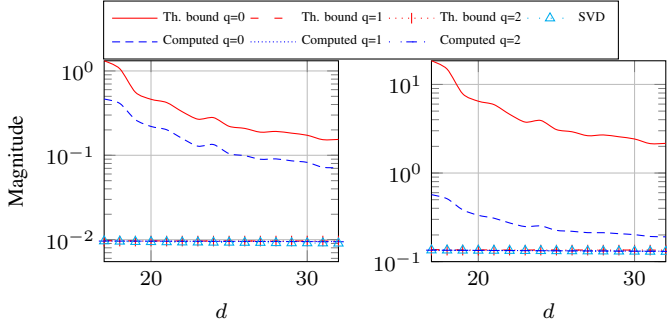


Fig. 21: \mathbf{P} -based low-rank approximation error for LowRankMediumGap. Left: Spectral norm. Right: Frobenius norm.

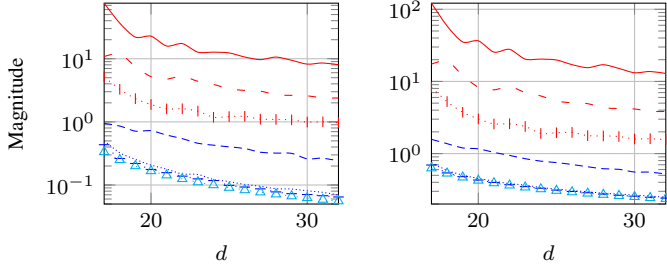


Fig. 22: \mathbf{P} -based low-rank approximation error for LowRankSlowDecay. Left: Spectral norm. Right: Frobenius norm.

The first line is due the truncation, see [22, Lemma 2.2], the second line is due to the optimality of the SVD, the third line is due to the triangle inequality, and the first term in the fourth line is due to (22). Inserting (26) into the last relation, the result follows. The second bound follows similarly. \square

APPENDIX F PROOF OF THEOREM 6

Owing to the statistical independence of Φ_1 and Φ_2 , we take expectations of the identity (11) in turn:

$$\begin{aligned} \mathbb{E}(\sigma_k(\mathbf{R}_{11})) &\geq \mathbb{E}_{\Phi_1} \left(\mathbb{E}_{\Phi_2} \left[\frac{\sigma_k}{\sqrt{1 + \delta_k^{4q+4} \|\Phi_2 \Phi_1^\dagger\|_2^2}} \right] \right) \\ &\geq \mathbb{E}_{\mathbf{G}_1} \left(\frac{\sigma_k}{\sqrt{1 + \delta_k^{4q+4} \eta_1^2 \|\mathbf{G}_1^\dagger\|_2^2}} \right) \geq \frac{\sigma_k}{\sqrt{1 + \delta_k^{4q+4} \eta^2}}. \end{aligned}$$

The second and third inequalities follow from Proposition 5.4 and Proposition 5.5 of [22], respectively.

To prove (12), the identity is first simplified to:

$$\|\mathbf{R}_{22}\|_{2,F} \leq \|\Sigma_\perp\|_{2,F} + \delta_k^{2q+1} \|\Phi_2 \Phi_1^\dagger\|_2 \|\Sigma_\perp\|_{2,F}.$$

We then take expectations in turn:

$$\begin{aligned} \mathbb{E}\|\mathbf{R}_{22}\|_{2,F} &\leq \mathbb{E}_{\Phi_1} \left(\mathbb{E}_{\Phi_2} \left[\|\Sigma_\perp\|_{2,F} + \delta_k^{2q+1} \|\Phi_2 \Phi_1^\dagger\|_2 \|\Sigma_\perp\|_{2,F} \right] \right) \\ &\leq \mathbb{E}_{\Phi_1} \left(\|\Sigma_\perp\|_{2,F} + \delta_k^{2q+1} \mathbb{E}_{\Phi_2} \left[\|\Phi_2 \Phi_1^\dagger\|_2 \right] \|\Sigma_\perp\|_{2,F} \right) \\ &\leq \mathbb{E}_{\Phi_1} \left(\|\Sigma_\perp\|_{2,F} + \delta_k^{2q+1} \left[\|\Phi_1^\dagger\|_F + \sqrt{m} \|\Phi_1^\dagger\|_2 \right] \|\Sigma_\perp\|_{2,F} \right) \\ &\leq \|\Sigma_\perp\|_{2,F} + \delta_k^{2q+1} \left[\sqrt{\frac{k}{p-1}} + \frac{e\sqrt{m(p+k)}}{p} \right] \|\Sigma_\perp\|_{2,F}. \end{aligned}$$

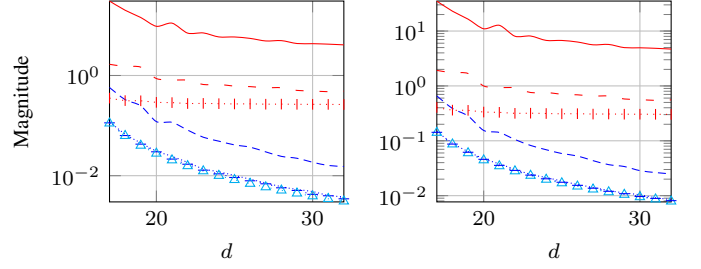


Fig. 23: \mathbf{P} -based low-rank approximation error for LowRankFastDecay. Left: Spectral norm. Right: Frobenius norm.

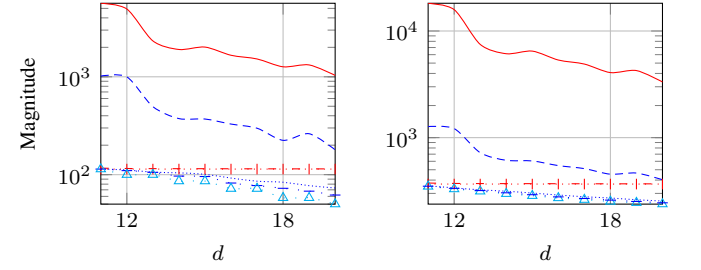


Fig. 24: \mathbf{P} -based low-rank approximation error for imppcol_e. Left: Spectral norm. Right: Frobenius norm.

The fourth line follows from [20, Proposition 10.1], and the last line from [20, Proposition 10.2] together with the Hölder's inequality: $\mathbb{E}_{\Phi_1} \|\Phi_1^\dagger\|_F \leq \left(\mathbb{E}_{\Phi_1} \|\Phi_1^\dagger\|_F^2 \right)^{1/2}$. \square

APPENDIX G PROOF OF THEOREM 7

To prove the first bound, by leveraging the statistical independence of Φ_1 and Φ_2 , we take expectations of the first identity over Φ_2 and Φ_1 :

$$\begin{aligned} \mathbb{E} \sin \theta_i &\leq \mathbb{E}_{\Phi_1} \left(\mathbb{E}_{\Phi_2} \left[\frac{\delta_i^{2q+2} \|\Phi_2 \Phi_1^\dagger\|_2}{\sqrt{1 + \delta_i^{4q+4} \|\Phi_2 \Phi_1^\dagger\|_2^2}} \right] \right) \\ &\leq \mathbb{E}_{\Phi_1} \left(\sqrt{\frac{\delta_i^{4q+4} \omega_1^2 \|\Phi_1^\dagger\|_2^2}{1 + \delta_i^{4q+4} \omega_1^2 \|\Phi_1^\dagger\|_2^2}} \right) \leq \sqrt{\frac{\delta_i^{4q+4} \omega_1^2 \omega_2^2}{1 + \delta_i^{4q+4} \omega_1^2 \omega_2^2}}. \end{aligned}$$

The second and third inequalities follow from Proposition 3 and Proposition 5 of [5], respectively. The second bound follows similarly. \square

REFERENCES

- [1] Q. Cao, Y. Pei, K. Akbudak, A. Mikhalev, G. Bosilca, H. Ltaief, D. Keyes, and J. Dongarra, "Extreme-scale task-based cholesky factorization toward climate and weather prediction applications," in *PASC '20*. New York, USA: Association for Computing Machinery, 2020.
- [2] L. Mor-Yosef and H. Avron, "Sketching for principal component regression," *SIAM J. Matrix Anal. Appl.*, vol. 40, no. 2, pp. 454–485, 2019.
- [3] J. Fan, K. Wang, Y. Zhong, and Z. Zhu, "Robust high dimensional factor models with applications to statistical machine learning," *Electronic Journal of Statistics*, vol. 36, pp. 303–327, 2021.
- [4] J. Jiang, J. Chung, and E. de Sturler, "Hybrid Projection Methods with Recycling for Inverse Problems," *SIAM J. Sci. Comput.*, vol. 43, no. 5, pp. S146–S172, 2021.
- [5] M. F. Kaloorazi and R. C. de Lamare, "Subspace-orbit randomized decomposition for low-rank matrix approximations," *IEEE Trans. Signal Process.*, vol. 66, no. 16, pp. 4409–4424, Aug 2018.

```

function [Q, L, P] = ru_qlp(A, k, p, q)
% This function computes the RU-QLP (Randomized-Unpivoted QLP) decomposition of A,
% where A is a general matrix of size mxn, with m>=n.
% Input arguments:
%   A: input data matrix
%   k: numerical rank of A, or a desired approximation rank.
%   p: oversampling parameter.
%   q: power iteration factor.
% Output arguments:
%   Q: an mxk matrix approximating range(A)
%   L: a dxk lower-triangular matrix whose diagonals approximate the singular values
%   P: an nxd matrix approximating range(A^T)
[m,~] = size(A);
d = k+p;
Phi = randn(m,d);
B = A*Phi;
[Pb,~] = qr(B,0);
for i = 1:q
    B = A*Pb; [Pb,~] = qr(B,0);
    B = A*Pb; [Pb,~] = qr(B,0);
end
[Q, R] = qr(A*Pb,0);
[Pt,Rt] = qr(R',0);
P = Pb*Pt; L = Rt';
return

```

```

function [Ur,Sr,Vr] = r_svd(A, k, p, q)
% Randomized SVD (R-SVD)
[~,n] = size(A);
d = k+p;
Omega = randn(n,d);
Y = A*Omega;
[Q,~] = qr(Y,0);
for i = 1:q
    Y = A*Q; [Q,~] = qr(Y,0);
    Y = A*Q; [Q,~] = qr(Y,0);
end
B = Q*A;
[UU,D,VV] = svd(B,'econ');
Ur = Q*UU;
Sr = D;
Vr = VV;
return
%[Ref] N. Halko, P.-G. Martinsson, and J. Tropp, "Finding structure with randomness:
% Probabilistic algorithms for constructing approximate matrix
% decompositions," SIAM Rev., vol. 53, no. 2, pp. 217-288, Jun. 2011.

```

```

function [Uc,Tc,Vc] = cor_utv(A, k, p, q, flag)
% Compressed Randomized UTU (CoR-UTU)
% If flag=0, the matrix D is approximated; if flag=1, D is computed.
[~,n] = size(A);
d = k+p;
C2 = randn(n,d);
for i = 1:q+1
    C1 = A*C2; Z = C2; % non-updated T2
    C2 = A*C1;
end
[Q1,~] = qr(C1, 0);
[Q2,~] = qr(C2, 0);
if flag == 0
    D_apprx = Q1'*C1*(pinv(Q2'*Z));
else
    D_apprx = Q1'*A*Q2;
end
[Qt,Rt,Pt] = qr(D_apprx);
Tc = Rt;
Uc = Q1*Qt;
Vc = Q2*Pt;
return
% [ref] M. F. Kaloorazi and R. C. de Lamare, "Compressed Randomized
% UTU Decompositions for Low-Rank Matrix Approximations," IEEE J. Sel.
% Topics Signal Process., vol. 12, no. 6, pp.1-15, Dec 2018.

```

```

function [U,D,V] = rp_tsod(A, k, p, q)
% Randomized Pivoted TSOD (RP-TSOD)
[m,~] = size(A);
d = k+p;
G = randn(m,d);
B = G*A;
[Q,~] = qr(B',0);
for i = 1:q
    B = A*Q; [Q,~] = qr(B,0);
    B = A*Q; [Q,~] = qr(B,0);
end
C = A*Q;
[Qc, Rc] = qr(C,0);
[Qrc,Rrc,Pr] = qr(Rc);
[Qh, Rh, Ph] = qr(Rrc');
U = Qc*Qrc*Ph;
D = Rh';
V = Q*Pr*Qh;
return
% [Ref] M. F. Kaloorazi and J. Chen, "Efficient low-rank approximation of matrices
% based on randomized pivoted decomposition," IEEE Trans. Signal Process.,
% vol. 68, pp. 3575-3589, Jun 2020.

```

```

function A = LowRankOneGap(n, LinSpa, k, mu)
% This function generates low-rank matrices
% with one gap in the spectrum.
d = linspace(1, LinSpa, n);
d(k+1:end) = 0;
G = randn(n);
[Qo,~] = qr(G);
G = G/(norm(G));
A = Qo*diag(d)*Qo' + mu*d(k)*G;
end

```

```

function A = LowRankPolyDecay(m, n, r, t)
% This function generates low-rank matrices with
% polynomially decaying spectrum.
p = min(m,n);
if m >= n
    [U, ~] = qr(randn(m,n),0);
    [V, ~] = qr(randn(n));
else
    [U, ~] = qr(randn(m));
    [V, ~] = qr(randn(n,m),0);
end
dr = ones(r,1)';
switch t
case 1
    d2 = (2:p-r+1).^(-1); % Slow polynomial decay
case 2
    d2 = (2:p-r+1).^(-2); % Fast polynomial decay
otherwise
    disp('Not a valid t value!');
    exit;
end
S = [dr d2];
A = U*diag(S)*V';
end

```

- [6] M. Adelman, K. Levy, I. Hakimi, and M. Silberstein, "Faster neural network training with approximate tensor operations," in *NeurIPS*, vol. 34, 2021, pp. 27 877–27 889.
- [7] Z. Shao, L. Landau, and R. C. de Lamare, "Dynamic Oversampling for 1-Bit ADCs in Large-Scale Multiple-Antenna Systems," *IEEE Trans. Commun.*, vol. 69, no. 5, pp. 3423–3435, May 2021.
- [8] E. Abbe, "Community Detection and Stochastic Block Models: Recent Developments," *JMLR*, vol. 8, pp. 1–86, 2018.
- [9] A. Buttari, M. Huber, P. Leleux, T. Mary, U. Rude, and B. Wohlmuth, "Block low-rank single precision coarse grid solvers for extreme scale multigrid methods," *Numer. Linear Algebra Appl.*, vol. 29, no. 1, p. e2407, 2022.
- [10] H. Cai, M. F. Kaloorazi, and J. Chen, "Online generalized eigenvectors extraction via a fixed-point approach," *IEEE Trans. Signal Process.*, vol. 69, pp. 2435–2451, Mar 2021.
- [11] T. T. Cai, Z. Ren, and H. H. Zhou, "Estimating structured high-dimensional covariance and precision matrices: Optimal rates and adaptive estimation," *Electron. J. Stat.*, vol. 10, no. 1, pp. 1–59, 2016.
- [12] J. Gardner, G. Pleiss, K. Q. Weinberger, D. Bindel, and A. G. Wilson, "Gpytorch: Blackbox matrix-matrix gaussian process inference with gpu acceleration," in *Adv. Neural Inf. Process. Syst.*, S. Bengio, H. Wallach, H. Larochelle, K. Grauman, N. Cesa-Bianchi, and R. Garnett, Eds. Curran Associates, Inc.
- [13] Y. Chen, C. Ma, H. Vincent Poor, and Y. Chen, "Learning mixtures of low-rank models," *IEEE Trans. Inf. Theory*, vol. 67, no. 7, pp. 4613–4636, Jul 2021.
- [14] G. H. Golub and C. F. van Loan, *Matrix computations*, 3rd ed., Johns Hopkins Univ. Press, Baltimore, MD, 1996.
- [15] T. F. Chan, "Rank revealing QR factorizations," *Linear Algebra and its Applications*, vol. 88-89, pp. 67–82, Apr 1987.
- [16] G. W. Stewart, "The QLP approximation to the singular value decomposition," *SIAM J. Sci. Comput.*, vol. 20, no. 4, pp. 1336–1348, 1999.
- [17] J. Demmel, L. Grigori, M. Gu, and H. Xiang, "Communication avoiding rank revealing QR factorization with column pivoting," *SIAM J. Matrix Anal. & Appl.*, vol. 36, no. 1, pp. 55–89, 2015.
- [18] J. Dongarra, M. Gates, A. Haider, J. Kurzak, P. Luszczek, S. Tomov, and I. Yamazaki, "The singular value decomposition: Anatomy of optimizing an algorithm for extreme scale," *SIAM Rev.*, vol. 60, no. 4, p. 808–865, 2018.
- [19] J. Dongarra, L. Grigori, and N. J. Higham, "Numerical algorithms for high-performance computational science," *Philosophical Transactions of the Royal Society A: Mathematical, Physical and Engineering Sciences*, vol. 378, no. 2166, p. 20190066, 2020.

- [20] N. Halko, P.-G. Martinsson, and J. Tropp, "Finding structure with randomness: Probabilistic algorithms for constructing approximate matrix decompositions," *SIAM Review*, vol. 53, no. 2, pp. 217–288, Jun 2011.
- [21] M. F. Kaloorazi and J. Chen, "Projection-based QLP algorithm for efficiently computing low-rank approximation of matrices," *IEEE Trans. Signal Process.*, vol. 69, pp. 2218–2232, Mar 2021.
- [22] M. Gu, "Subspace iteration randomization and singular value problems," *SIAM J. Sci. Comput.*, vol. 37, no. 3, pp. A1139–A1173, 2015.
- [23] M. F. Kaloorazi and R. C. de Lamare, "Compressed randomized UTV decompositions for low-rank matrix approximations," *IEEE J. Sel. Topics Signal Process.*, vol. 12, no. 6, pp. 1–15, Dec 2018.
- [24] A. K. Saibaba, "Randomized subspace iteration: Analysis of canonical angles and unitarily invariant norms," *SIAM J. Matrix Anal. & Appl.*, vol. 40, no. 1, p. 23–48, Jan 2019.
- [25] M. F. Kaloorazi and J. Chen, "Randomized truncated pivoted QLP factorization for low-rank matrix recovery," *IEEE Signal Processing Letters*, vol. 26, no. 7, pp. 1075–1079, Jul 2019.
- [26] —, "Efficient low-rank approximation of matrices based on randomized pivoted decomposition," *IEEE Trans. Signal Process.*, vol. 68, pp. 3575–3589, Jun 2020.
- [27] G. W. Stewart, *Matrix algorithms: volume 1: basic decompositions*, SIAM, Philadelphia, PA, 1998.
- [28] Y. P. Hong and C.-T. Pan, "Rank-Revealing QR Factorizations and the Singular Value Decomposition," *Math. of Comput.*, vol. 58, no. 197, pp. 213–232, Jan 1992.
- [29] S. Chandrasekaran and I. C. F. Ipsen, "On rank-revealing QR factorizations," *SIAM J. Matrix Anal. & Appl.*, vol. 15, no. 2, pp. 592–622, 1994.
- [30] A. Björck, *Numerical methods in matrix computations*. Texts in Applied Mathematics vol. 59, Springer Cham, 2015.
- [31] D. A. Huckaby and T. F. Chan, "On the convergence of Stewart's QLP algorithm for approximating the SVD," *Numerical Algorithms*, vol. 32, pp. 287–316, 2003.
- [32] A. Buttari, J. Langou, J. Kurzak, and J. Dongarra, "A class of parallel tiled linear algebra algorithms for multicore architectures," *Parallel Computing*, vol. 35, no. 1, pp. 38–53, 2009.
- [33] R. M. Larsen, *Efficient Algorithms for Helioseismic Inversion*, PhD Thesis, University of Aarhus, Denmark (1998).
- [34] R. D. Fierro, P. C. Hansen, and H. P. S. K., "UTV Tools: Matlab templates for rank-revealing UTV decompositions," *Numerical Algorithms*, vol. 20, pp. 165–194, 1999.
- [35] C. Musco and C. Musco, "Randomized Block Krylov Methods for Stronger and Faster Approximate Singular Value Decomposition," in *NIPS*, 2015, pp. 1396–1404.
- [36] Q. Yuan, M. G. and B. Li, "Superlinear convergence of randomized block lanczos algorithm," in *IEEE ICDM*, 2018, pp. 1404–1409.
- [37] J. A. Tropp, "Randomized block Krylov methods for approximating extreme eigenvalues," *Numer. Math.*, vol. 150, pp. 1217–255, 2022.
- [38] P.-G. Martinsson and S. Voronin, "A randomized blocked algorithm for efficiently computing rank-revealing factorizations of matrices," *SIAM J. Sci. Comput.*, vol. 38, no. 5, pp. S485–S507, 2016.
- [39] J. A. Duersch and M. Gu, "Randomized projection for rank-revealing matrix factorizations and low-rank approximations," *SIAM Rev*, vol. 62, no. 3, pp. 661–682, 2020.
- [40] V. Rokhlin, A. Szlam, and M. Tygert, "A randomized algorithm for principal component analysis," *SIAM J. Matrix Anal. & Appl.*, vol. 31, no. 3, pp. 1100–1124, 2009.
- [41] A. Gittens and M. W. Mahoney, "Revisiting the Nyström method for improved large-scale machine learning," *JMLR*, vol. 17, pp. 1–65, 2016.
- [42] J. Tropp, A. Yurtsever, M. Udell, and V. Cevher, "Practical Sketching Algorithms for Low-Rank Matrix Approximation," *SIAM J. Matrix Anal. & Appl.*, vol. 38, no. 4, pp. 1454–1485, 2017.
- [43] N. Chepurko, K. L. Clarkson, P. Kacham, and D. P. Woodruff, "Near-optimal algorithms for linear algebra in the current matrix multiplication time," in *SODA*, 2022, pp. 3043–3068.
- [44] J. L. Barlow, "Block modified gram–schmidt algorithms and their analysis," *SIAM J. Matrix Anal. & Appl.*, vol. 40, no. 4, pp. 1257–1290, 2019.
- [45] B. C. Gunter and R. A. Van De Geijn, "Parallel out-of-core computation and updating of the qr factorization," *ACM Trans. Math. Softw.*, vol. 31, no. 1, pp. 60–78, Mar. 2005.
- [46] T. Joffrain, M. L. Tze, E. S. Quintana-Ortí, R. van de Geijn, and F. Van Zee, "Accumulating Householder transformations, revisited," *ACM Trans. Math. Softw.*, vol. 32, no. 2, pp. 169–179, Jun. 2006.
- [47] N. Wu and H. Xiang, "Randomized QLP decomposition," *Linear Algebra and its App.*, vol. 599, p. 18–35, Aug 2020.
- [48] S. Wang, Z. Zhang, and T. Zhang, "Improved analyses of the randomized powermethod and block Lanczos method," *arXiv:1508.06429v2*, 2015.
- [49] P. Drineas, I. C. F. Ipsen, E.-M. Kontopoulou, and M. Magdon-Ismail, "Structural convergence results for approximation of dominant subspaces from block krylov spaces," *SIAM J. Matrix Anal and Appl.*, vol. 39, no. 2, pp. 567–586, 2018.
- [50] Y. Nakatsukasa and N. Higham, "Stable and efficient spectral divide and conquer algorithms for the symmetric eigenvalue decomposition and the SVD," *SIAM J. Sci. Comput.*, vol. 35, no. 3, p. A1325–A1349, 2013.
- [51] R. Mathias and G. W. Stewart, "A block QR algorithm and the singular value decomposition," *Linear Algebra and its App.*, vol. 182, pp. 91–100, 1993.
- [52] A. Björck and G. H. Golub, "Numerical methods for computing angles between linear subspaces," *Math. Comp.*, vol. 27, pp. 579–594, 1973.
- [53] P. Zhu and A. V. Knyazev, "Angles between subspaces and their tangents," *J. Num. Math.*, vol. 21, no. 4, pp. 325–340, 2013.
- [54] T. Davis and Y. Hu, "The University of Florida Sparse Matrix Collection," *ACM Trans. Math. Softw.*, vol. 38, no. 1, pp. 1–25, 2011.
- [55] C. Paige and M. Wei, "History and generality of the cs decomposition," *Linear Algebra and its App.*, vol. 208–209, pp. 303–326, 1994.
- [56] G. Stewart, "A generalization of saad's theorem on rayleigh–ritz approximations," *Linear Algebra and its App.*, vol. 327, no. 1, pp. 115–119, 2001.
- [57] Y. Nakatsukasa, "Accuracy of singular vectors obtained by projection-based svd methods," *Bit Numer Math*, vol. 57, p. 1137–1152, 2017.
- [58] R. A. Horn and C. R. Johnson, *Matrix analysis*, 2nd ed., Cambridge Univ. Press, 2012.
- [59] D. S. Bernstein, *Matrix Mathematics: Theory, Facts, and Formulas - Second Edition*. Princeton University Press, 2 edition, 2009.
- [60] G. W. Stewart and J.-g. Sun, *Matrix perturbation theory*, Academic Press 1990.